POLITECNICO
MILANO 1863

SCUOLA DI INGEGNERIA INDUSTRIALE
E DELL'INFORMAZIONE

The Octopus Robot: From Biological Principles to a Soft Robotic System for Coordinated Multi-Arm Underwater Grasping

Tesi di Laurea Magistrale in
Mechanical Engineering - Ingegneria Meccanica

Author: **Andrea Mirabelli**

Student ID: 247413
Advisor: Giovanni Bianchi
Co-advisors: Barbara Mazzolai, Emanuele Solfiti
Academic Year: 2025-26

Abstract

Exploration and manipulation in harsh, unstructured underwater environments represent a significant challenge for traditional rigid grippers. These scenarios frequently require grasping of complex-shaped objects and dexterous manipulation of delicate species, areas in which Bio-inspired Soft Robotics offers a promising alternative, leveraging natural biological principles and intrinsic material compliance to ensure high adaptability and safe physical interactions. Among marine organisms, the octopus serves as an exceptional biological model for advanced underwater grasping; however, existing literature primarily focuses on the optimization of single-arm systems. Starting from the single arm design developed at the *Italian Institute of Technology*, this work introduces a novel multi-arm architecture. This transition is motivated by the need to explore cooperative manipulation strategies and more complex interaction scenarios, that exceed the functional limits of a single manipulator. The design process began with a biological investigation in *Acquario di Genova*, where new manipulation strategies were observed and characterized. Based on these observations, a soft robotic gripper integrating three distinct arms was developed, featuring passive suckers and tendon-driven actuation, with two different, tailored tendon configurations. The project involved a comprehensive development process, spanning from the initial mechanical design, its fabrication and the implementation of dedicated control strategies. An extensive experimental validation was conducted in both air and water, to assess the effectiveness of the bio-inspired strategies. The results demonstrate that the multi-arm configuration significantly enhances payload capacity, showing an improvement of over 400% compared to single-arm systems, justifying the increased system complexity. It also exhibits superior performance in underwater environments, confirming it as the ideal operating medium, with a 34.3% increase in payload capacity with respect to dry conditions. These findings show the potential of cooperative octopus-inspired soft arms for advanced, safe, and effective real-world marine applications.

Keywords: Soft Robotics; Bio-inspired Robotics; Underwater Grasping; Tendon-driven Actuators; Octopus-inspired Robotic Arms

Abstract in lingua italiana

L'esplorazione e la manipolazione in ambienti sottomarini ostili e non strutturati rappresentano una sfida significativa per i rigidi gripper tradizionali. Tali scenari richiedono la presa di oggetti dalla geometria complessa e la manipolazione di specie fragili, ambiti nei quali la robotica soffice bio-ispirata offre un'alternativa promettente, sfruttando principi biologici naturali e la deformabilità intrinseca dei materiali per garantire elevata adattabilità e interazioni fisiche sicure. Tra gli organismi marini, il polpo costituisce un modello biologico eccezionale per la manipolazione sottomarina; tuttavia, la letteratura esistente si concentra sull'ottimizzazione di sistemi a singolo braccio. Partendo dal design del singolo braccio sviluppato presso l'*Istituto Italiano di Tecnologia*, questo lavoro introduce un'architettura multi-braccio. Tale transizione è motivata dalla necessità di esplorare strategie di manipolazione cooperativa e scenari di interazione più complessi, che superano i limiti funzionali di un manipolatore singolo. Il processo di progettazione è iniziato con un'indagine biologica condotta presso l'*Acquario di Genova*, dove nuove strategie di manipolazione sono state osservate e caratterizzate. Sulla base di tali osservazioni è stato sviluppato un gripper robotico soffice composto da tre bracci, dotati di ventose passive e attuazione a tendini. Il progetto ha previsto uno sviluppo completo, dalla progettazione meccanica iniziale alla fabbricazione e all'implementazione di strategie di controllo. Un'estesa validazione sperimentale è stata condotta in aria e in acqua per valutare l'efficacia delle strategie bio-ispirate. I risultati dimostrano che questa configurazione incrementa significativamente la capacità di carico, con un miglioramento superiore al 400% rispetto ai sistemi a singolo braccio, giustificando la maggiore complessità del sistema. Inoltre, il sistema mostra prestazioni superiori in ambiente acquatico, con un aumento della capacità di carico del 34,3% rispetto alle condizioni in aria. Tali risultati mostrano il potenziale di bracci soffici cooperativi ispirati al polpo per applicazioni marine reali, sicure ed efficaci.

Parole chiave: Robotica Soffice; Robotica Bio-ispirata; Manipolazione Sottomarina; Attuazione a Tendini; Bracci Robotici Ispirati al Polpo

Contents

Abstract **1**

Abstract in lingua italiana **3**

Contents **5**

1 Introduction **7**

2 Bio-inspired Soft Robotics **9**
2.1 Bio-inspired Robotics 9
2.2 Soft Robotics 10

3 State of the Art: Underwater Grippers **11**
3.1 Rigid Grippers and Manipulators 11
3.2 Soft Grippers 13
3.3 Octopus-inspired Robotic Arms 17

4 Biological Investigation: Characterization of Octopus' Grasping Strategies **23**
4.1 Motivations and Scientific Background 23
4.2 Experimental Methodology and Setup 27
4.3 Results 29

5 Soft Arm Design, Fabrication, and Characterization **37**
5.1 Design and Fabrication 37
5.2 Experimental Characterization 41

6 Multi-Arm Octopus Robot **47**
6.1 Mechanical Design 48
6.2 Control Strategies 56

7 Experimental Validation and Results **61**
7.1 Framework and Workspace 61
7.2 Grasping Performance 64

8 Conclusions **77**

Bibliography **79**

Acknowledgements **89**

1 | Introduction

The exploration of marine environments and the execution of dexterous manipulation tasks present significant technological challenges, especially in the physical interaction with delicate organisms and complex, unstructured scenarios. Traditionally, underwater manipulation has been performed using rigid robotic grippers deployed on Remotely Operated Vehicles (ROVs). While highly effective for heavy-duty industrial operations, these conventional grippers struggle to adapt to irregular geometries. The lack of intrinsic compliance makes them inherently unsuitable for handling fragile marine species, where excessive localized pressure can easily damage the target.

In recent years, soft robotics has emerged as a highly promising alternative, offering intrinsic safety and adaptability. By using highly compliant materials, soft manipulators can safely conform to the target's shape, drastically reducing the risk of damage and the computational cost. However, maximizing payload capacity and grasping stability without sacrificing this intrinsic compliance remains an open challenge for the deployment of soft grippers in demanding underwater scenarios. Nature offers highly optimized solutions to overcome these engineering challenges. The octopus is an exceptional example of advanced manipulation capabilities, relying on a completely soft body to navigate, hunt, and interact with objects of various sizes and shapes. The soft robotics community has derived extensive inspiration from the octopus; however, previous studies and developed prototypes have focused almost exclusively on the kinematics and performance of a single octopus-inspired arm. At the *Italian Institute of Technology*, the research in this field is highly advanced, and the present work takes the single arm design developed here as the baseline for the enhancements. These single-arm manipulators successfully replicate bending and wrapping motions, enabling versatile and effective grasping, but they are limited in their overall payload and grasping stability. The physical coordination and cooperative manipulation strategies of multiple octopus-inspired arms, remains an approach that has never been systematically designed and tested in robotics, highlighting a fundamental area for further technological advancement.

The primary objective of this work is to bridge this gap by designing, developing, and

validating a novel bio-inspired robotic system, specifically engineered for the underwater grasping of delicate and complex-shaped targets. Taking direct inspiration from the biological strategies observed during dedicated experiments with the octopi, conducted in *Acquario di Genova*, this research introduces a multi-arm architecture and investigates its effectiveness in performing different grasping strategies.

The contributions of this work are systematically detailed throughout the manuscript, which is organized as follows:

- **Chapter 2** introduces the fundamental concepts of Bio-inspired Soft Robotics, highlighting its key advantages.
- **Chapter 3** reviews the state of the art in underwater manipulation, offering a critical comparison between rigid and soft grippers, and providing a comprehensive overview of octopus-inspired robotic technologies.
- **Chapter 4** details the biological investigation conducted in *Acquario di Genova*. By observing the animal interacting with objects of various shapes and sizes, this study extracted key kinematic principles regarding multi-arm coordination. The observations led to the formal characterization of two distinct bio-inspired grasping strategies: *Pinching* and *Basal Grasping*. Understanding these natural mechanisms provided the crucial design guidelines for the robotic prototype.
- **Chapter 5** focuses on the design, fabrication, and experimental characterization of the single soft arm. It describes the manufacturing process of the silicone structure, the integration of different tendon routings and the evaluation of their kinematic capabilities, providing fundamental information for the design of the multi-arm platform.
- **Chapter 6** presents the overall design of the Multi-Arm Octopus Robot. It provides a comprehensive overview of its mechanical design, electronic architecture, and control strategies, detailing the specific motivations and objectives driving each engineering choice.
- **Chapter 7** discusses the extensive experimental validation and the results of the grasping performance tests. It offers a comparative analysis between different configurations (1 arm, 3 arms, different tendon pulling percentage, different grasping strategies) both in air and water, effectively validating the bio-inspired strategies applied to different objects.

2 | Bio-inspired Soft Robotics

Traditional robotics, based on the use of rigid links and joints, has achieved remarkable results in structured and controlled environments, where robot tasks and environmental reactions are pre-established with a high degree of precision. However, as robots are increasingly required to operate in unstructured, dynamic, and unpredictable real-world scenarios, such as underwater exploration [20], search and rescue operations [44], human interaction and medical applications [52], the limitations of systems designed following this traditional approach become evident [30]. To overcome these challenges, researchers have looked towards nature for solutions. Over millions of years of evolution, biological organisms have developed highly efficient strategies for movement, perception, and object manipulation in complex environments [3].

2.1. Bio-inspired Robotics

Bio-inspired robotics is an interdisciplinary field that applies biological principles to the design and control of engineering systems. It is not limited to the simple mimic of living organisms, but rather it studies the underlying functional mechanisms that guarantee biological systems their performances [47]. The translation of biological features into robotic systems offers several key advantages:

- **Adaptability:** Biological systems can adapt to changing and harsh environments, often never experienced before. Bio-inspired robots aim to replicate this versatility, allowing to deal with new scenarios without complete reprogramming or hardware redesign from scratch [48].
- **Energy Efficiency:** Animals have evolved locomotion and grasping strategies that exploit the dynamic interaction between their bodies and the environment (e.g., exploiting passive dynamics or elastic energy storage) to minimize energy consumption [10].
- **Functional Integration:** In nature, there is rarely a clear separation between structure, actuation, and perception. Bio-inspired design leads to highly integrated

systems where the mechanical structure itself facilitates control and perception.

2.2. Soft Robotics

Soft Robotics represents a paradigm shift from the traditional approach, that is based on rigid links and discrete joints [30, 33]. It involves instead the use of soft materials, such as elastomers, silicones, and gels (Young's modulus $< 10^6$ Pa), to build robots capable of continuous deformation [51]. This approach is inspired by soft-bodied organisms (e.g., cephalopods, caterpillars, worms) or soft organs (e.g., the elephant trunk [34]), which possess a theoretically infinite number of degrees of freedom (DOFs).

A fundamental concept in soft robotics is "Embodied Intelligence": in rigid robots, "intelligence" is typically centralized in the control algorithm. In soft robots, part of the computational load is transferred to the mechanical properties of the physical body itself [47]. The material properties (elasticity, viscosity, density) and morphology allow the robot to passively adapt to the environment, simplifying control requirements; indeed, an active control system is often not required during grasping. Conversely, traditional robots require precise geometric modeling of the object they intend to grasp, precise trajectory planning, and grasping force control.

The intrinsic compliance of soft robots offers a series of advantages over their rigid counterparts:

- **Safe Interaction:** Soft robots can safely interact with delicate objects or humans. In case of a collision, the body deforms, absorbing the impact energy and avoiding damage to both the robot and the target.
- **Conformability:** The ability to deform allows soft robots to passively adapt their body around objects of complex and, above all, unknown geometry [32]; this allows these systems to work in environments with low or even absent visibility, without the need for complex video systems or 3D scanners to study the object's geometry. They are also able to squeeze into confined spaces that would be inaccessible to rigid structures.
- **Resilience:** Soft materials make these robots highly robust to mechanical impacts, falls, or environmental hazards that would otherwise damage rigid structures.

Despite these advantages, Soft Robotics presents notable engineering challenges that constitute the current frontier of research: controllability, accuracy, and effectiveness are still challenging tasks [62], and also design and fabrication are non-trivial aspects.

3 | State of the Art: Underwater Grippers

The capability to physically interact with the marine environment is a fundamental requirement for the advancement of modern underwater robotics. While early underwater vehicles were primarily designed for observation and data collection, current applications, ranging from biological sampling and archaeological recovery to the maintenance of offshore infrastructure, require systems capable of flexible and safe interventions [25].

Underwater grasping poses unique challenges compared to terrestrial manipulation. The environment is unstructured, dynamic, and hostile, characterized by high pressures, low temperatures, and significant disturbances such as ocean currents [56]. Furthermore, visibility is often compromised by turbidity and light absorption, complicating the visual feedback necessary for teleoperation or autonomous control [25, 35]. In this context, the design of the end-effector plays a critical role. It serves as the physical interface between the robot and the external world, determining the success of the manipulation task. The following sections analyze the different categories of underwater grippers, classifying them into rigid, soft bio-inspired, and octopus-inspired solutions, with a particular focus on their suitability for interacting with delicate and irregular objects [40].

3.1. Rigid Grippers and Manipulators

Historically, underwater manipulation has been dominated by rigid-body robotic systems. These manipulators, typically mounted on Remotely Operated Vehicles (ROVs) or Autonomous Underwater Vehicles (AUVs) (Figure 3.1), are designed as kinematic chains of rigid links connected by rotary or prismatic joints [56]. They represent the industry standard for deep-sea interventions due to their reliability, high payload capacity, and positioning precision.

Rigid underwater manipulators are generally classified based on their actuation method: hydraulic or electric. Hydraulic systems are prevalent in ROVs used for heavy-duty tasks,

as they offer a high power-to-weight ratio and are naturally robust against high pressure [56]. Electric manipulators, on the other hand, are becoming increasingly popular for smaller vehicles due to their cleaner operation, higher energy efficiency, and more precise control capabilities [56].

While traditional end-effectors were limited to simple two-finger ("parallel-jaw") grippers or intermeshing claws, recent research has pushed towards multi-fingered, cable-driven designs to enhance dexterity and workspace [64]. For example, underactuated three-fingered grippers have been developed (Figure 3.2), capable of executing both parallel and precision grasps on objects of variable dimensions [5, 6]. These designs often use tendon transmissions to house sensitive electronics and motors inside watertight chambers, decoupling them from the wet environment.

From a control perspective, these systems are often teleoperated using a Master-Slave approach, where the operator moves a "master" arm from the sea surface, and the underwater "slave" arm replicates the motion. This architecture has proven to be effective even for small-sized modular robotic arms designed for inspection-class ROVs [4].

However, effective manipulation requires reliable feedback. Therefore, given the limitations of vision in turbid waters, the integration of tactile feedback is crucial. Advanced rigid grippers now incorporate 6-axis force/torque sensors directly in the wrist or fingertips to allow for autonomous grasp regulation [46]. The development of such sensors presents significant engineering challenges, particularly regarding the selection of sealing materials (e.g., silicone, rubber) to ensure performance under high hydrostatic pressure [45].

Despite these advances, rigid manipulators face significant limitations when interacting with unstructured environments or delicate objects [18]. The major limitation is their intrinsic rigidity. If contact forces are not perfectly regulated, the stiff interface can easily crush fragile biological specimens or damage archaeological artifacts [40].

To mitigate this issue, some intermediate solutions, such as the "Ocean One" robot hand (Figure 3.1), have introduced mechanical compliance through spring-loaded transmissions [59]. This adaptive design allows the fingers to absorb impacts and conform better to objects.

Figure 3.1: The Girona 500 AUV platform with its arm and gripper. Reprinted from [5].

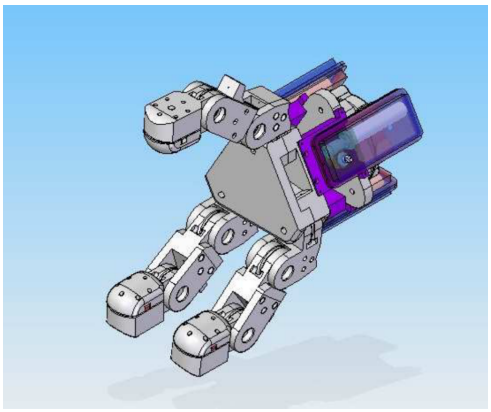

Figure 3.2: Detail of the three-fingered rigid end-effector: CAD view of the actuation mechanism. Reprinted from [6].

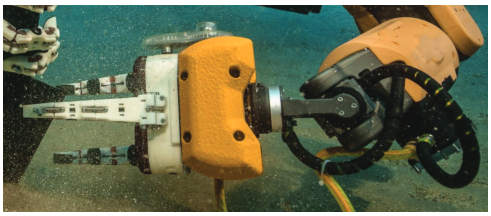

Figure 3.3: Execution of a grasp on a tubular object by the "Ocean One" hand. Reprinted from [59].

However, the mechanical complexity of such systems remains high, and the ability to wrap around complex objects is limited compared to the solutions found in the soft robotics field [60].

3.2. Soft Grippers

In response to the limitations of rigid manipulators, the scientific community has progressively adopted soft robotics solutions for delicate underwater interaction. Interest in this field has grown over the years (Figure 3.4), further supported by the increasing attention shown by companies.

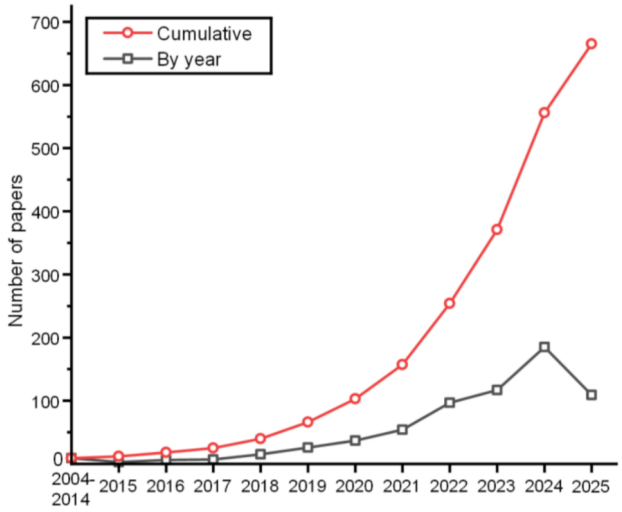

Figure 3.4: Number of publications per year from Google Scholar in August 2025. The search terms were <Bionic> AND <Soft Grippers> AND <Underwater>.

The choice of actuation technology is a determinant factor for the performance of a soft system, influencing force, response speed, and controllability. In literature, soft actuators for underwater applications are classified into three main categories: fluidic actuators, cable-driven (tendon-driven) actuators, and actuators based on smart materials [17, 51].

- **Fluidic Elastomer Actuators (FEAs):** This is the most widespread category for underwater manipulation due to its intrinsic safety and the possibility of using the surrounding water as the operating fluid. They are subdivided into:
  - **Pneumatic Networks (PneuNets):** Composed of a series of internal air chambers that expand when pressurized. Their asymmetric arrangement forces the actuator to bend. They are easy to fabricate but require relatively low pressures to avoid rupture [50].
  - **Fiber-Reinforced Actuators:** These utilize inextensible threads (e.g., Kevlar or Nylon) wrapped around an elastomer body. The orientation of the fibers guides the deformation (elongation, torsion, or bending) and allows operation at much higher pressures compared to PneuNets, generating greater forces suitable for deep-sea applications [20].
  - **McKibben Muscles:** Known as pneumatic artificial muscles (PAMs), they consist of an internal air chamber enclosed in a braided sheath. When pressurized, they shorten and expand radially, mimicking biological muscle contraction with a high force-to-weight ratio [67].

  - **Bellows-type:** These utilize a pleated structure (origami or accordion style). They are ideal when large linear extensions or wide bending angles are required with low activation pressures [63].

- **Tendon-Driven Actuation:** "Cable-driven" or "Tendon-driven" actuators use inextensible cables sliding inside a soft matrix (silicone) or along defined guides. Tensioning of the cable causes the shortening of the side where it slides, generating bending or twisting. This approach mimics, for example, the longitudinal muscles of octopus arms [31]. This system allows motors (heavy and sensitive to water) to be placed in a watertight chamber far from the end-effector, leaving the part in contact with the environment completely soft and lightweight [14].

- **Smart Materials:** Although less common for high-force applications, they offer compact solutions without moving mechanical parts.

  - **Shape Memory Alloys (SMA):** Alloys (e.g., Nitinol) that recover their original shape when heated (typically by Joule effect). They were used in early prototypes of octopus arms to generate silent and biological contractions [15]. However, slow cooling in air limits their operating frequency, preventing the execution of rapid and frequent activation cycles, although the underwater environment helps dissipate heat faster.

  - **Dielectric Elastomer Actuators (DEAs):** Polymers that deform under high electric voltage. They offer very fast response times (similar to muscles) but require dangerously high voltages (> 1 kV) to operate in saltwater [17].

Unlike traditional systems, soft grippers are made of intrinsically soft materials, allowing passive adaptation to the shape of the target object [26]. This approach exploits the principle of "impedance matching": to safely interact with soft biological organisms (such as corals, sponges, or jellyfish), the robot's stiffness must be comparable to that of the organism itself.

A fundamental example is represented by grippers developed for deep-sea sampling (Figure 3.6), which use 3D-printed silicone pneumatic fingers to gently wrap around samples ("form closure") without exerting damaging point pressures [20]. For even more critical manipulations, such as capturing jellyfish, "ultragentle" actuators reinforced with nanofibers have been developed, capable of exerting extremely low contact pressures (< 1 kPa), demonstrating the superiority of soft grasping in preserving the structural and genetic integrity of organisms [53].

A key advantage of soft grippers is the speed and accessibility of fabrication processes.

It has been demonstrated that it is possible to design and 3D print molds for actuators directly on board oceanographic vessels ("shipboard fabrication"), allowing researchers to adapt the gripper morphology in real-time based on the organisms encountered during the mission [63]. Furthermore, the design approach is shifting towards "User-Driven" methodologies, which directly involve marine biologists in the design loop to ensure that the gripper meets real versatility requirements, such as the ability to collect both biological samples and marine litter with the same end-effector [49]. The effectiveness of these designs is increasingly supported by non-linear FEM (Finite Element Method) modeling, which allows predicting complex elastomer deformations and optimizing gripper topology before fabrication [24].

Although compliance is advantageous, excessive softness can limit payload capacity or grasp stability. To overcome this limitation, recent research has introduced variable stiffness mechanisms. An effective technique is "granular jamming": by filling a soft geometry with granular particles and applying a vacuum, it is possible to transition from a flexible to a rigid state, significantly increasing grasp robustness and resistance to sharp or pointed objects [70]. Another strategy involves the use of bio-inspired Rigid-Soft hybrid designs. An example of this is a gripper inspired by the lobster claw (*Homarus americanus*), which integrates small rigid "teeth" on the soft surface of the fingers [29]; this hybrid texture improves friction and grasp stability on slippery underwater objects, surpassing the performance of purely smooth surfaces.

Additionally, to handle objects of widely varying sizes, bionic grippers with "variable effective length" have been proposed (Figure 3.5), which, by modulating internal pressure, can change the active portion of the finger, adapting to both small debris and large samples [23].

Finally, the integration of these soft manipulators into mobile platforms, such as benthic legged robots [36], has provided the basis for new forms of "Underwater Mobile Manipulation," extending the workspace and enabling complex operations directly on the seabed.

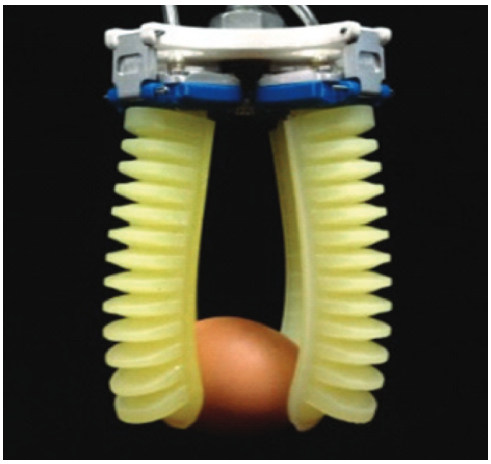

Figure 3.5: Soft Bionic gripper with variable effective length, grasping an egg. Reprinted from [23].

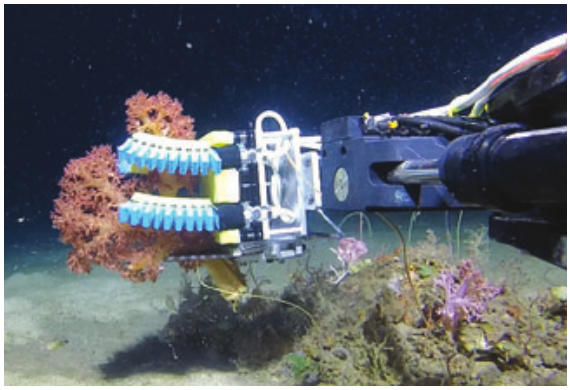

Figure 3.6: Bellows-type gripper collecting soft coral. Reprinted from [20].

3.3. Octopus-inspired Robotic Arms

Among marine organisms, the octopus represents an ideal biological model for soft robotics, thanks to its exceptional capabilities of manipulation, locomotion, and adaptation to narrow spaces, all in the absence of a rigid skeleton. This invertebrate sea animal, specifically a cephalopod, is a paradigmatic example of an animal with high motor capabilities and intelligent behavior. The motor capabilities of its arms are far beyond any existing robot, for their dexterity and for the variability of their stiffness. This enhanced behavior and capability of interaction with the environment is due to the peculiar morphology of the octopus's body, especially to the form and materials of its arms, and their efficient distributed neural control. From a robotic engineering point of view, the octopus and its arms present peculiar characteristics [16], that can be summarized as:

- **Infinite number of DOFs**
- **Bending in all directions, at any point along the arm**
- **Variable and controllable stiffness**
- **Locomotion and manipulation capabilities, with the same non-specialized arms**
- **Highly distributed control**

The research conducted at the *Italian Institute of Technology* (*IIT*) and the *Scuola Superiore Sant'Anna*, has deeply analyzed the biomechanics of this cephalopod, to extract

the fundamental engineering principles [31, 41].

The key characteristic of the octopus arm is its muscular structure, defined as a "Muscular Hydrostat". In the absence of rigid parts, structural support is provided by the resistance to compression of the internal volume, which remains constant: a contraction in one dimension, necessarily causes an expansion in another [37]. This architecture is organized into three main muscle groups:

- **Longitudinal muscles:** They run along the arm axis and are responsible for shortening and, if activated asymmetrically, for bending.
- **Transverse muscles:** Arranged perpendicularly to the axis, their contraction reduces the arm diameter causing elongation.
- **Oblique muscles:** They wrap around the arm spirally and control twisting.

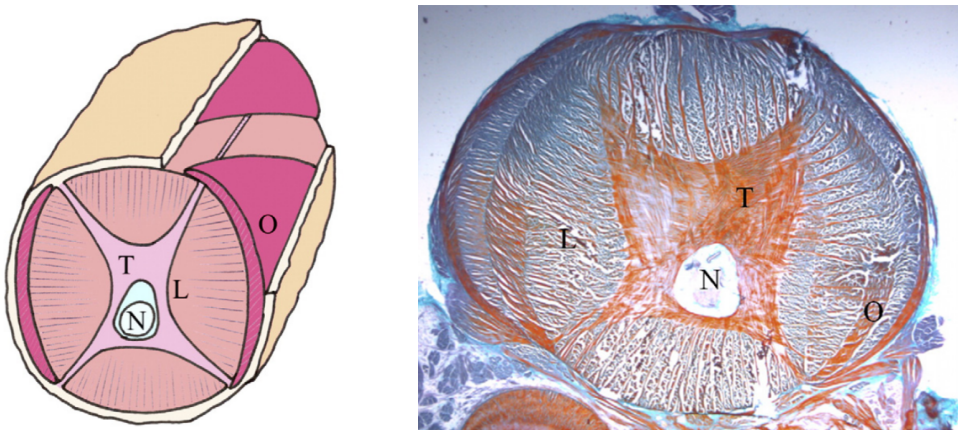

(a) (b)

Figure 3.7: Octopus arm sections. Schematic drawing (a) and histological picture (b): (O) oblique, (T) transverse and (L) longitudinal muscles; (N) nerve cord. Images reprinted from [15].

The combined contraction of these muscles (the transverse and longitudinal muscles can be considered to have a reciprocal antagonistic action) allows the octopus to selectively stiffen the arm ("stiffening") to apply force, while remaining intrinsically soft [15]. This phenomenon is a perfect example of "Embodied Intelligence", where the mechanical properties of the physical body facilitate control and interaction with the environment, reducing the computational load [16]. Furthermore, the performances achieved by the octopus in terms of elongation and force are sensational: the octopus arm can elongate by 70% and one arm alone exhibits an average pulling force of 40 N [37].

Applying the basic principles of this smart muscle arrangement to build an artificial muscular hydrostat is one of the key aspects of the design of octopus-inspired arms in research. In robots, the different muscles are reproduced by cables, routed inside the soft external structure ("tendon driven actuation").

Several international research groups have attempted to replicate the grasping capabilities of the octopus, using different technological approaches, often focusing on specific subsets of movements or alternative materials. Bezha et al. [8] demonstrated that the low complexity of the design and control of their proposed continuum soft octopus-inspired manipulator, make it a powerful tool for object manipulation in complex environments. Other materials have also been tested [27] (sponge and rubber); they have shown that the grasping of unknown objects could be realized by the dynamics of the body without complex control signals. Although these systems succeed in achieving grasps in all anatomical planes (ventral, dorsal, lateral, and torsional), their force capacity and precision remain limited. On the front of smart materials, Ye et al. [68] proposed a flexible manipulator actuated entirely by Shape Memory Alloy (SMA) wires. Despite the elegance of the solution, that doesn't need bulky motors, the system must face challenges related to the complex mathematical modeling of large deformations and the thermal response times of SMAs.

More recently, Wu et al. [65] presented the "Glowing Sucker Octopus Gripper", inspired by the deep-sea species *Stauroteuthis syrtensis*. This hybrid design uses a 3D-printed linkage mechanism to actuate an umbrella-like membrane, integrating modular soft suckers. Although effective for grasping irregular objects, the use of internal rigid links partially deviates from the concept of a purely soft manipulator, introducing kinematic constraints that are not present in the biological model.

At the *Italian Institute of Technology* (*IIT*), extensive research has been conducted on octopus-inspired arms, leading to the development of numerous prototypes, that evolved from early experimental versions to robust tools for real-world applications. This research line is part of the framework of the RAISE project (Robotics and AI for Socio-economic Empowerment), funded by the European Union as part of the National Recovery and Resilience Plan (NRRP), which aims to translate these bio-inspired technologies into concrete solutions for the service and industrial sectors.
Early works focused on the replication of the muscular hydrostat, integrating longitudinal cables (for shortening and bending) and transverse SMA springs (for diameter variation and so elongation) inside silicone matrices [15, 31]. With these, the stiffening mechanism through co-contraction was validated. The most significant evolution towards industrial application is represented by the soft arm with integrated suction cups [42]. This arm

has a thin conical shape, optimized to work in confined environments (such as pipes) and is actuated by longitudinal cables only. A vacuum system is added to activate the suckers, distributed on the ventral surface. The system is capable of generating high grasping forces (up to 12.5 times greater in oil compared to friction alone) and operating in pressurized environments up to 18 bar. Furthermore, the suction cups allow to grasp objects that would escape a simple coiling grasp, enabling hybrid grasping modes (suction and friction combined). Currently, the research is exploring "soft proprioception", through the integration of distributed sensors, such as optical fibers (FBG) and inertial systems (IMU), directly into the silicone body [38]. This step is fundamental to pass from open-loop to closed-loop control, allowing the robot to reconstruct its pose even in the absence of visual feedback, a typical condition of deep ocean. Finally, the optimization of cable routing via genetic algorithms and FEM reconstructions, is allowing for a reduction in the number of actuators required (without sacrificing dexterity), which constitutes a critical aspect for the scalability of the system [39].

Figure 3.8: Arm with active suckers grasping a cylindrical object (20mm diameter). Reprinted from [43].

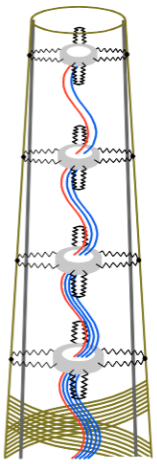

Figure 3.9: The SMA modules and the braid layers of the arm developed by Cianchetti et al. [16].

In addition to manipulation, octopus morphology has inspired robots capable of locomotion, and sometimes multimodal locomotion (crawling and swimming). Some exploit the octopus swimming mechanism [69], by adding a quick-return mechanism to maximize thrust during swimming. Others have explored the use of multiple materials with variable stiffness to improve synchrony and hydrodynamic efficiency during underwater swimming [1]. Furthermore, hybrid systems exist, combining manipulation and locomotion [66]. A pioneering example is the “PoseiDrone” [2], which has crawling, swimming,

and manipulation abilities, designed to operate on rough seabeds. Beyond manipulation, the robot combines "crawling" (walking on the seabed by using arms) and pulsed-jet thrusters propulsion, mimicking the jet-propulsion swimming system of cephalopods.

Despite the remarkable progress, underwater soft grippers still present significant limitations and open challenges. Modeling and control of soft continuum bodies is a complex task, because unlike rigid robots with discrete joints, soft arms possess virtually infinite degrees of freedom, making standard kinematic approaches computationally expensive and often inaccurate due to the non-linear behavior of hyper-elastic materials. This complexity is further amplified by the fact that effective proprioceptive sensing is still an active area of research. Estimating the exact pose of a deformable arm without external visual feedback (often compromised in turbid waters) remains an open challenge.
Furthermore, a fundamental trade-off exists between compliance and payload capacity. While softness ensures safety and adaptability, it also limits the force exertable by the end-effector, restricting the variety of objects that can be effectively handled. Finally, the most significant gap, and the specific focus of the present work, is the transition from single-arm to multi-arm operations. While octopuses rely on the synergistic use of multiple arms to stabilize, manipulate, and transport objects, the robotic counterparts operate as isolated units. In an underwater environment, a single soft arm often struggles to secure a stable grasp on floating or suspended objects: without a rigid backbone or an opposing force, the target tends to be pushed away or displaced rather than grasped. Developing strategies to accommodate multiple soft actuators for cooperative grasping represents the necessary step to bridge the gap between biological efficiency and robotic implementation.

4 | Biological Investigation: Characterization of Octopus' Grasping Strategies

4.1. Motivations and Scientific Background

To design a multi-arm robotic system, it is first necessary to have a solid knowledge of the strategies that the octopus uses to coordinate its eight arms. As discussed in Section 3.3, the scientific literature has extensively analyzed the motor capabilities of the single octopus arm, defining precise kinematic and dynamic models. However, the transition from the control of a single arm to the coordination of multiple ones for complex manipulation tasks remains a less explored area, especially from a robotics-oriented perspective. This section summarizes some specific knowledge on octopus psychobiology and neurophysiology, highlighting above all, the gaps that motivated the experimental campaign conducted in *Acquario di Genova*.

Scientific studies have identified that, despite the infinite number of degrees of freedom, the octopus simplifies motor control using "stereotypical patterns". Fundamental studies conducted by Sumbre et al. [61] and Hanassy et al. [22] allowed for the decomposition of the octopus's complex mobility into a set of movements:

- **Reaching:** This is the movement used to extend the arm toward a target (Figure 4.1a). It has been demonstrated that this does not occur through a simple uniform extension, but through the propagation of a curvature wave ("bend propagation") that travels from the base toward the tip, pushing the arm toward the target [61]. Subsequent studies have integrated this model, highlighting how reaching is often a combination of this wave and pure axial elongation [22].
- **Fetching:** To bring food to the mouth after grasping, the octopus adopts a different kinematic strategy, configuring the soft arm into a "quasi-articulated structure" (Figure 4.1b). By selectively stiffening specific sections of the arm (thus creating

temporary "elbows"), the octopus executes a point-to-point rotational movement, surprisingly similar to that of human articulated arms [61].

- **Twisting:** To wrap around an object, the octopus gives the arm a spiral shape, with the suckers facing internally, toward the object (Figure 4.1c).

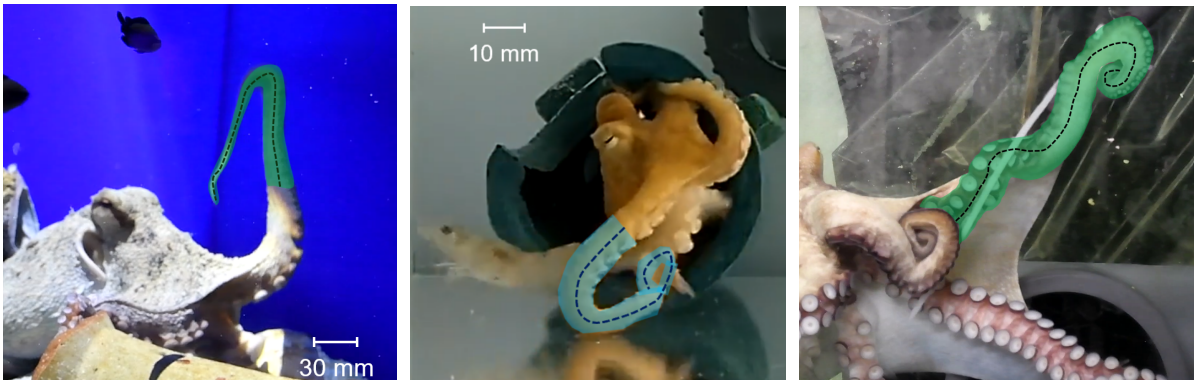

(a) (b) (c)

Figure 4.1: Octopus arm movements: (a) Reaching, (b) Fetching and (c) Twisting. Figure (b) is adapted from [9], figures (a) and (c) are taken from videos recorded for this work.

These movements are fundamental both from a control perspective and for understanding the types of movement available to the octopus, comparing them with the simplified ones obtained in the design (Chapter 5).

Regarding the octopus's decisional choices, several aspects must be taken into account, in preparation for the experiments. In exploration scenarios or in the absence of visual feedback, the arm adopts "blind" search behaviors, where movement is locally guided by the chemotactile sensors of the suckers ("chemotactile exploration"), adapting to the substrate roughness [54, 55]. During the exploration of complex environments, the octopus relies almost exclusively on these sensors, activating the suckers as soon as they come into contact with a surface. Indeed, suckers are not just actuators, but complex sensory organs capable of chemoreception and tactile discrimination [11, 12].

Recent studies, as the one by Gendreau et al. [21], have started to analyze how the octopus recruits additional arms ("neighboring arms") to manipulate hidden objects. A significant preference in the engagement of anterior arms was detected (Figure 4.2), with a maximum number of arm involved of 3/4/5 on average (Figure 4.3).

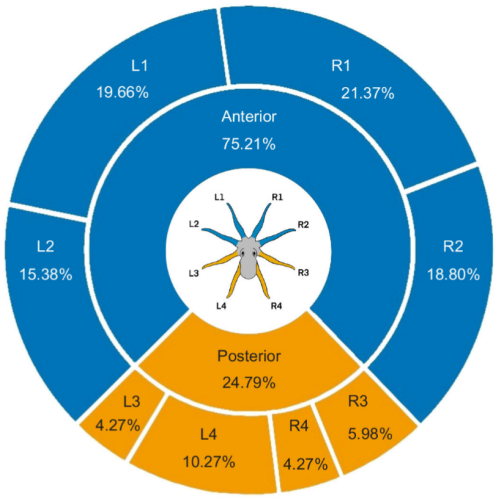

Figure 4.2: Occurrences (in percentage) in which each arm was engaged as first arm, to manipulate hidden objects. Reprinted from [21].

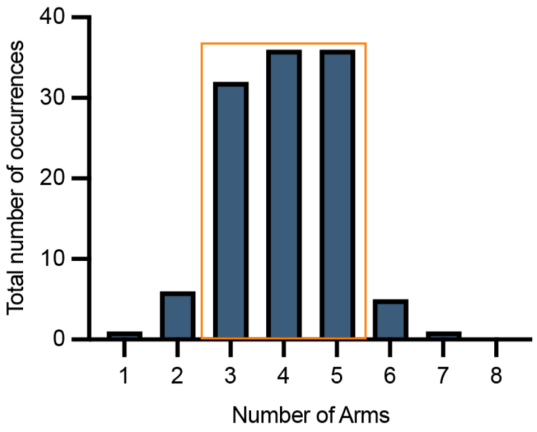

Figure 4.3: Maximum number of arms used simultaneously to manipulate hidden objects. Reprinted from [21].

However, two main problems arise regarding the interpretation of these results:

- These tests are designed to isolate and study decision-making factors in conditions of no direct visual contact with the object.
- These tests are not aimed at a study of object manipulation (intended as grasping typology or interaction with the object in space), but rather they are designed to study every choice that temporally precedes the manipulation.

The use of vision is left available to the octopus only in cases where one wants to specifically study how this sense influences the choice of arms to use, as for Byrne et al. [13]; in any case, the two problems mentioned above are not resolved simultaneously.

In the present experimental campaign, it was decided to remove all these aspects, already studied in literature, from the variables. For this reason, the objects will not be hidden behind domes, so, to the octopus will be allowed a clear view of the object; in this way, it will be possible to focus on the study of free object manipulation, without any constraint on the number of arms used and the senses available. This approach represents a major novelty in octopus' behavior investigation, as it combines a study in a controlled but open environment, with the study of manipulation from a robotics perspective.

Despite the progress in understanding the single arm and sensory mechanisms, a significant gap exists in literature regarding multi-arm cooperative manipulation strategies.

What is missing is an engineering classification of how the octopus decides to grasp an object, especially when a single arm is not sufficient.

For this work, a collaboration between *IIT* and *Acquario di Genova* has been established, providing access to a controlled environment and specialized biological expertise for the investigation.

The aim of the experiments was to study these aspects of octopus interaction:

- Grasping strategies (meaning the configuration of the arms during the grasping action, that defines a type of grasp; NOT to be confused with the set of simplified arm actions, like reaching, fetching and twisting).
- Number of arms used and their relative position on the object.
- Role of each arm during a grasping action (meaning if there is a subdivision of tasks between the different arms).
- Presence of collisions between arms and possible avoidance strategies.
- Actual manipulation of the object (how it's moved in space, how it's transferred between arms).
- Any errors in the grasping action and the reason for them.

Of all recorded interactions, particular attention will be given to those actions in which more than one arm is engaged.

Each of these features is evaluated in relation to the:

- size of the object (described in 4.2)
- distance from the object
- movement of the object
- number of objects grasped together

With the data obtained, it's expected to:

- Develop a design suitable for a multi-arm system (such as number of arms, size, and length).
- Select the most suitable relative position between the arms of the robot (such as distance and orientation).
- Implement control strategies to achieve the different types of poses and grasps.

In the following sections will be described the experimental procedure, the setup and the results derived from the collected data.

4.2. Experimental Methodology and Setup

The tests consisted of providing the octopuses in the aquarium with objects to interact with, stimulating their exploration and manipulation. The examined octopuses belong to 3 different species:

- *Enteroctopus dofleini (or "Giant pacific octopus")*: it is the largest known octopus species in the world, with arms that can exceed 3 m (with a total radial span of up to 6 m).
- *Octopus vulgaris*: it is the most common octopus of the Mediterranean Sea; its arms are around 1 m long.
- *Octopus maya*: a tropical species, with arms 1 m long.

The data from the different species will be initially analyzed separately, highlighting specific differences between them; however, a unified statistical analysis will be subsequently performed (Section 4.3), as a separate study for each species falls outside the scope of this work.

The objects used for the interactions were:

- Plastic jar (4.4a)
- Sponge balls (4.4b)
- Polypropylene rope (4.4c)
- Plastic sticks
- Food (prawns, shrimp, crabs)

The experiments consisted of placing these objects in the tank, within the octopus's field of view, and waiting for interaction to occur. To stimulate interaction, the objects were usually externally coated with food odors; for the jars, it was also possible to place food inside, thus forcing the octopus to perform a more complex interaction (unscrewing the cap and extracting the food from the inside). The rope was used to lower specific objects into the tanks.

(a) Plastic Jar: 7,1 x 8,5 *cm* (diameter x height)

(b) Sponge Balls 7 *cm* (diameter)

(c) Polypropylene Rope 10*mm* x 10*m* (diameter x length)

Figure 4.4: Objects used during the experiments.

The experimental tasks were not only functional for data collection but also served as a source of cognitive enrichment during feeding. By engaging the animal in problem-solving activities, the tests promoted its physical and psychological well-being, in accordance with the welfare guidelines for cephalopods in research [19].

The feeding regime was not altered during this period of tests, so was suitable with the lifestyle, natural diet and developmental stage of the animals. Thanks to these modalities, it was possible to avoid any form of stress caused to the animals.

The tests were recorded to extract the objective data. The videos were acquired using a camera setup composed of a Nikon D7500 and Logitech Brio webcams, to ensure a complete view of the animal from different angles and maintain visual contact even during movements toward the edges of the tanks. As the three different octopus species are housed in 3 different environments, it was necessary to employ 3 different setups:

- *Enteroctopus dofleini*: tank dimensions 420x220x280*cm*; given the size of the aquarium, it was necessary to use one Nikon D7500 and two Logitech Brios webcam, positioned at a distance of 1.60m from the frontal glass (Figure 4.5).
- *Octopus vulgaris*: tank dimensions 260x80x100*cm*; one Nikon and one Logitech were used, positioned at a distance of 1.10m from the frontal glass (Figure 4.6).
- *Octopus maya*: tank dimensions 120x80x80*cm*; one Nikon and one Logitech were used, positioned at a distance of 0.80m from the frontal glass (Figure 4.7).

Figure 4.5: Camera setup for the tank of *Enteroctopus dofleini*.

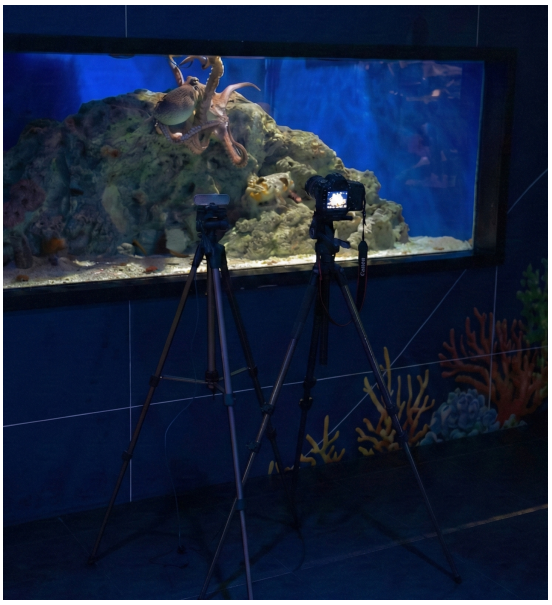

Figure 4.6: Camera setup for the tank of *Octopus vulgaris*.

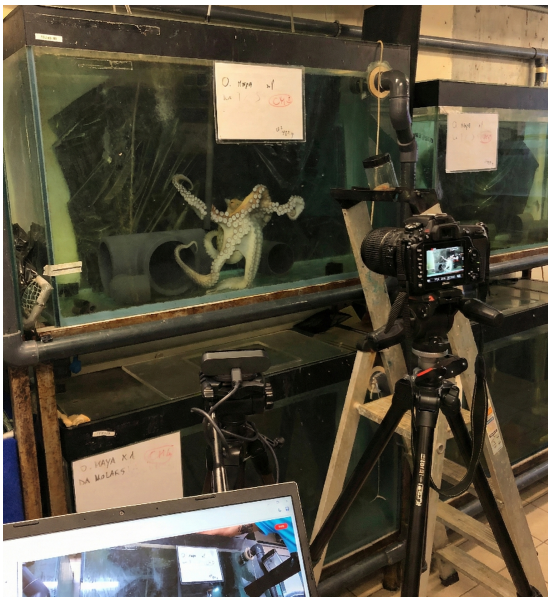

Figure 4.7: Camera setup for the tank of *Octopus maya*.

4.3. Results

From a total of 10 hours of recordings, 128 grasping actions were extracted and analyzed. From these data, it was possible to generate statistics regarding the number of arms used and also to discover and describe two new grasping strategies, never reported before.

Number of arms used

By initially considering the octopus species and objects separately, graphs were obtained (Figure 4.8) showing the frequency with which the octopus recruited a specific number of arms, to grasp the different objects (plastic jar, sponge balls, plastic sticks, food). Here are reported the graphs specific for the *Octopus maya* species.

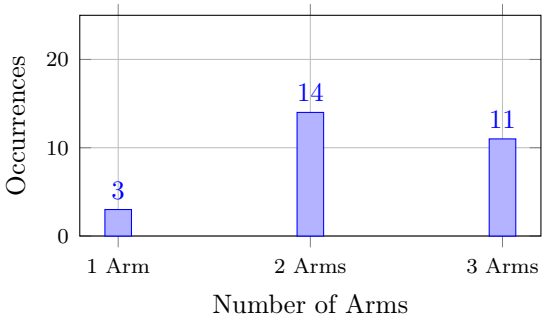

(a) Plastic stick: arm recruitment

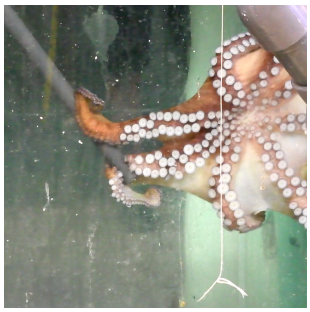

(b) Plastic stick: representative frame

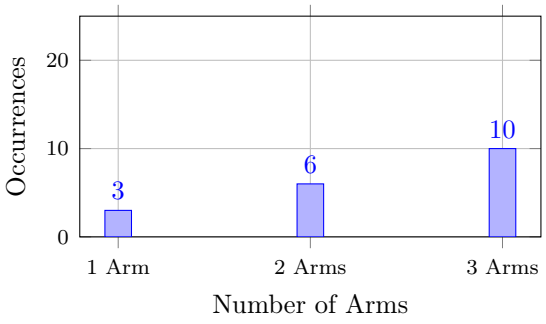

(c) Plastic jar: arm recruitment

(d) Plastic jar: representative frame

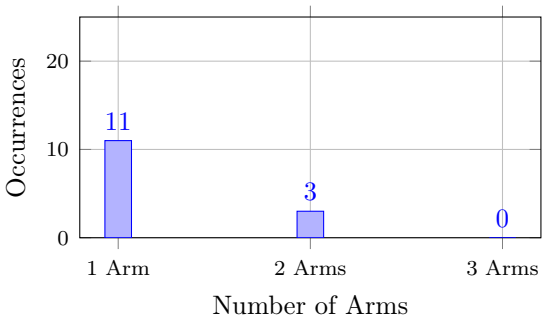

(e) Food: arm recruitment

(f) Food: representative frame

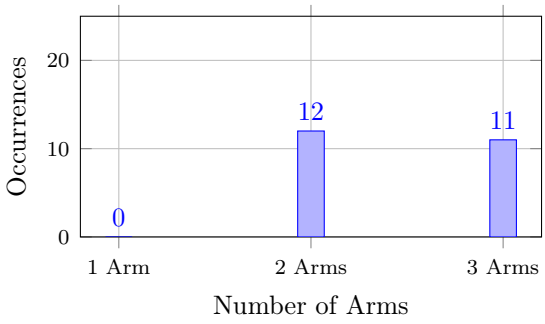

(g) Sponge ball: arm recruitment

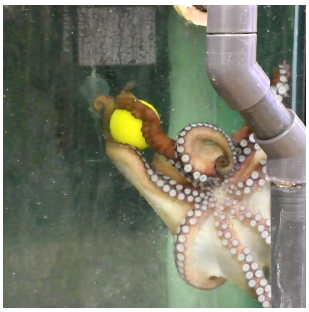

(h) Sponge ball: representative frame

Figure 4.8: Comparative analysis of arm recruitment during the grasping of different objects. Left column shows the frequency distribution (Histograms 4.8a, 4.8c, 4.8e, 4.8g); Right column shows representative frames (Figures 4.8b, 4.8d, 4.8f, 4.8h).

A surprising data can be observed: grasping attempts involving more than 3 arms have never been performed. The use of a limited number of arms, was attributed to two reasons:

- the remaining arms are used to stabilize the body, maintaining contact with the surrounding environment (Figure 4.9).
- this number of arms is sufficient to establish contact with the entire surface of the object, without arm overlap.

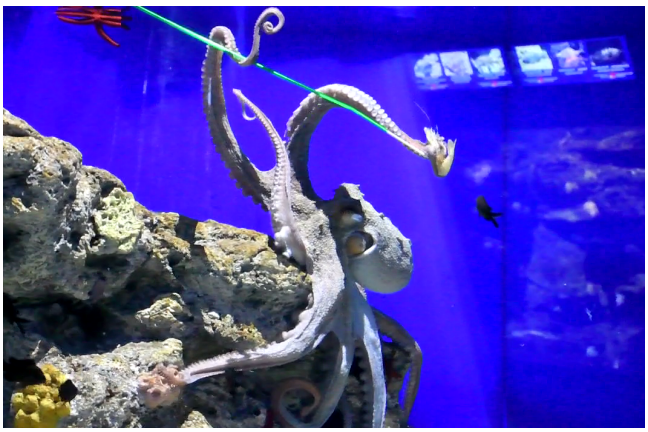

Figure 4.9: *Octopus vulgaris* using 2 arms for the grasping of a thin plastic stick with attached some food at the extremity, and keeping 5 arms in contact with the ground.

An exception to this behavior occurs when the octopus brings the object completely under its mantle ("parachute attack" [7]) so using all the arms to incorporate it; however, this behavior is not of interest for the purposes of this work, which focuses on manipulation.

To interact with long and cylindrical objects (Histogram 4.8a, Figure 4.8b), the octopus predominantly uses 2 or 3 arms, employing a grasping strategy that will be analyzed in the following paragraph; rarely it uses one single arm. The same applies to jars (Histogram 4.8c, Figure 4.8d), with a bigger tendency towards the use of 3 arms, to better stabilize a small object to which fewer suckers have the space to adhere.

In the "food" histogram, grasps where the arms enter in contact only with the food itself are counted. For this object typology (Histogram 4.8e, Figure 4.8f), a clear tendency emerges toward the use of a single arm (using the "fetching" strategy described previously in 4.1), with some exceptions involving 2 arms.

Finally, for spherical objects, such as sponge balls used here (Histogram 4.8g, Figure 4.8h), single-arm interactions were never recorded, neither with stationary nor with moving balls; the tendency here is to use the arms to wrap around the spherical object along two opposite semicircumferences (Figure 4.8h).

By performing the same count on the extracted highlights of the videos for the other octopus species, a summary table can be built (Table 4.1), where each cell reports the number of arms used most frequently:

	Dofleini	***Vulgaris***	***Maya***
Plastic stick	2	2/3	2
Plastic jar	2/3	3	3
Food	X	1	1
Sponge ball	3	X	2/3

Table 4.1: Summary table reporting the number of arms used most frequently. The nomenclature n/m is used when the statistical data for n arms and m arms have a difference ≤ 2 occurrences.

It can be noted that the species behave roughly in the same way when facing the same objects; as already explained for the *Octopus maya* above, a two-arms grasp is the most frequent for plastic sticks; for food, the use of a single arm prevails; for plastic jars and spherical objects instead, the use of three arms is predominant. The two "X" marks in the table indicate two different situations: for the species *Enteroctopus dofleini*, manipulation of food alone has never been recorded, because the animal always interacted with the

stick used to dip the food into the tank, to ensure a more stable grip; for the species *Octopus vulgaris*, no interaction with a sponge ball has ever been recorded, as the animal showed no interest in exploring this object. In general, more interactions were recorded for the *Octopus maya* compared to the other two species, due to their greater tendency to interact with objects, emerged during this study; this cannot be taken as a statistically significant finding because it may be caused by various environmental factors and factors relating to the individual specimen.

If the different objects and different octopuses are considered together, creating a unified statistic, a clear tendency to use 2 or 3 arms emerges (Figure 4.10).

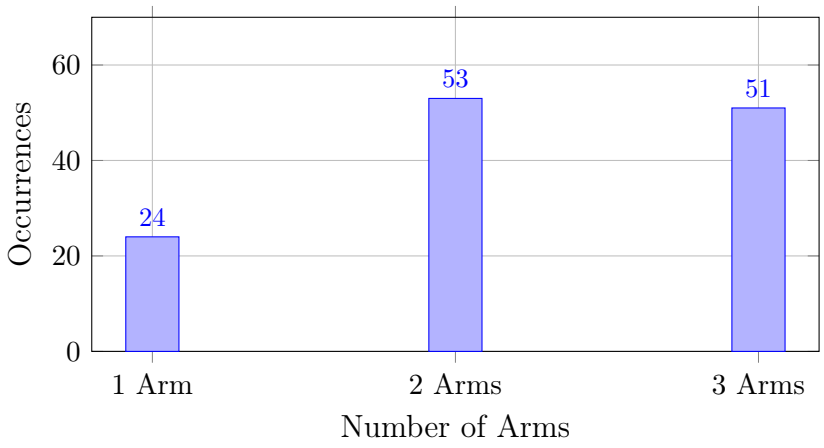

Figure 4.10: Overall distribution of the number of arm recruited, for the 3 species and all the objects together.

Comparing this graph with the graph shown previously (Figure 4.3), it can be observed that, compared to the case of manipulation of hidden objects, the number of arms used for grasping visible objects in water is, on average, lower. Two possible reasons for this difference have already been illustrated above; to these, one can add the fact that, thanks to the use of vision, a larger number of arms is not required to optimally explore the environment and the object. Furthermore, the use of a single arm is more relevant here with respect to the case without vision, but this is mainly due to the fetching movement performed with food.

This graph is crucial for the choice of the number of arms used for the robot developed in this work, as will be explained in Chapter 6.

New grasping strategies

By analyzing the video recordings, it was also possible to identify 2 new grasping strategies, not currently present in literature. They were named:

- ***Pinching:*** this grasping strategy is used to grasp long objects (plastic sticks, in this case) with the use of 2 arms, which are placed in contact with the object along its entire length (Figure 4.11); the arms are kept straight and the suckers are oriented internally, toward the object. This strategy is used to grasp objects that have their axis oriented in any direction (parallel to the axis of the octopus's body, perpendicular to the axis of the octopus's body, or any other). All the examined species performed this type of grasp (Figure 4.11, 4.12a, 4.12b).

Figure 4.11: *Octopus maya* performing pinching.

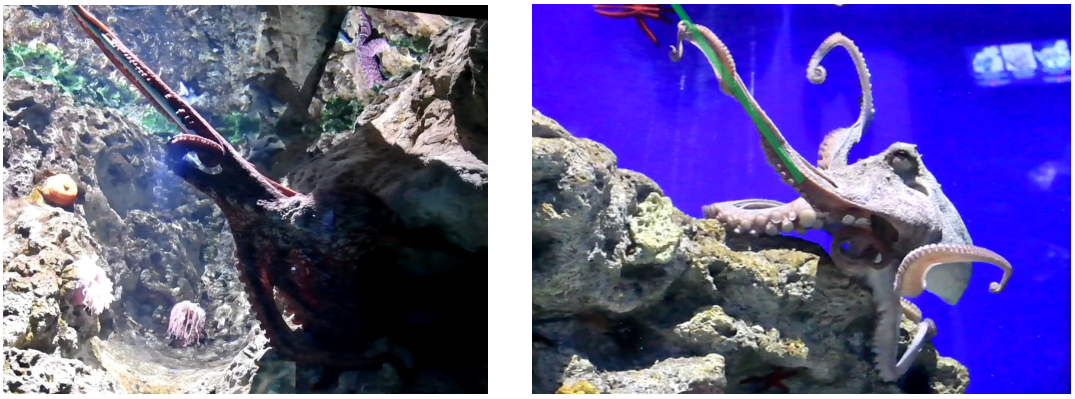

(a) (b)

Figure 4.12: Pinching strategy performed by *Enteroctopus dofleini* (a) and *Octopus vulgaris* (b). In (b), the object is hidden behind the arms, so a green transparent box is superimposed to highlight its position.

Thanks to this arm arrangement, the grip on the object is very strong, as the two arms compress the object and all the suckers can adhere, being in contact with the surface.

- ***Basal Grasping:*** this grasping strategy is used to grasp objects whose axis is oriented perpendicularly to the axis of the octopus's body (Figure 4.13); the grasp consists in the use of 3 arms with active suckers, facing inward (2 on one side and 1 on the other), which come in contact with the object at the basal part of the arm, very close to the body.

Figure 4.13: *Octopus maya* performing basal grasping of a plastic stick. The green dashed line represent the axis of the object, while the orange cross represent the axis of the object, pointing inside the plane.

With this grasping strategy, the octopus is able to maintain a stable grip on objects that tend to move away from the body in a direction parallel to the body axis.

These experiments should not be interpreted as pure behavioral experiments on the octopus, but rather as experiments conducted from a robotics perspective. Fundamental data were extracted and subsequently translated into design choices (such as number of arms, position, orientation, movements of individual arms, reciprocal movements to recreate the identified grasps, and control), as will be described in Chapter 5 and Chapter 6.

It is not excluded that, by collecting further data in the future, other grasping typologies may be discovered and analyzed.

To address the remaining objective questions of the study, it is important to mention that:

- A lack of interest in grasping multiple objects simultaneously has been observed.
- Difficulties emerged in grasping fast-moving objects (failed grasp), such as the sponge balls used while rising rapidly toward the surface (Figure 4.14); the coordination necessary to grasp objects at this speed resulted to be insufficient; a reason for this could be that the diet of these individuals does not include preys that perform rapid movements.
- In the described grasping types, the arms play an interchangeable, symmetrical role.

(a) (b) (c)

Figure 4.14: Frames of a failed grasp of a sponge ball. In (a) the ball is thrown towards the *Octopus maya*; in (b) the octopus tries to extend the arms to catch it; in (c) the arms are not wrapped around the ball, it goes up towards the surface.

5 | Soft Arm Design, Fabrication, and Characterization

5.1. Design and Fabrication

The octopus-inspired soft robotic arms are fabricated by curing Ecoflex™ 00-30 silicone material in a 3D-printed two-part mould. This material is selected for its exceptional softness and ease of use: Ecoflex is a silicone elastomer with low stiffness (5 kPa – 80 kPa), highly flexible and deformable; it shows characteristics such as biocompatibility, relatively low cost, chemical resistance, and adaptability to dynamic loading and environmental conditions [28]. The softness of Ecoflex is specified by its Shore hardness, which typically ranges from 00-20 to 00-50. For this work, the 00-30 version was selected, since its mechanical properties closely mimic those of a real octopus arm [43].

The arms were fabricated starting from a mould designed at IIT, therefore the shape was not a design variable (the design variables are explained below); the resulting arm has a conical shape, with a diameter of 40 mm at the base, a total length from base to tip of 410 mm, and a conicity of 2.22° (Figure 5.5).

On the ventral side, there are 10 suckers, but it is important to specify that:

- The suckers are passive, meaning that is not possible to generate an artificial suction pressure inside them. Their working principle relies on physical compression: when pressed against an object, the fluid inside the cavity is expelled, creating a pressure drop that enables adhesion.
- The suckers attach passively to objects (only in water), and this will influence the tests, as will be explained in Chapter 7.

The adoption of passive suckers is driven by two main reasons:

- **Simplicity of design:** active suckers require a complex pneumatic system, which must be integrated into the design of both the actuation system and the silicone arm itself [43].

- **Investigation of "shape-based" grasping:** since this is the first study addressing the transition from a single-arm to a multi-arm system of octopus-inspired arms, it was decided to start with this type of grasping alone, without the help of active suckers, to study the basic interactions between multiple arms and objects.

The arms are actuated using flexible cables (tendons), routed through internal channels within the silicone body, and anchored in precise positions along the arms.

The tendons employed are commercial braided fishing lines (Spiderwire, DuraBraid [58]); these cables are composed of Dyneema (Ultra-High Molecular Weight Polyethylene - UHMWPE) microfibers, a material selected for its excellent mechanical properties. Unlike monofilament nylon, this braided structure exhibits negligible elongation (near-zero stretch), ensuring immediate force transmission and precise position control without elastic hysteresis. Additionally, the cables feature a fluoropolymer coating that significantly reduces the friction coefficient.

The tendons are each one connected to a dedicated servo motor, located in a remote actuation unit. When a motor applies tension to a cable, the resulting shortening generates a compressive force along the arm's longitudinal axis, causing the soft structure to bend or curl towards the actuated side. This approach allows for the delocalization of heavy components, such as motors, keeping the gripper lightweight and compliant, as explained in Section 3.2.

The design variables were:

- **Cable arrangement ("tendon routing"):** depending on the configuration of the cables within the silicone body, the movements obtained after curing are different.
- **Internal supports:** the ends of the wires are anchored to these, enabling the application of forces inside the arm, and thus movements. There are different methods for positioning and fixing them: an endoskeleton can be used (Solfiti et al. [57]), that enables tendons to be placed through predefined holes, before the silicone casting phase; to minimize its impact on the overall stiffness of the soft body, the endoskeleton was designed with a slim profile, flexible connections, and 3D-printed with elastic material (Shore A hardness 50), selected to roughly match the mechanical properties of the surrounding silicone matrix. Alternatively, internal supports can be used, which become part of the mould [38].

In this work, a method belonging to the family of internal supports was adopted, using custom supports. They are made of 3D printed PLA and can be mainly divided into two types: the first type (Figure 5.1) has the shape of an annular disk, with eyelets equally

distributed along the circumference; it has a cylindrical protrusion, which is inserted inside the mould before the silicone casting phase, to keep its position fixed, and thus maintain the cables in the correct position during curing. The second type (Figure 5.2) has a geometry similar to the first, but lacks the protrusion for fixation, therefore requiring it to be fixed in position with dedicated cables, attached to the mould. The advantage of this second type is that it leaves smaller holes on the external surface of the silicone arm, at the cost, however, of increased time required for positioning and removal. Both types were tested, and for the final versions of the arms, both were used, in alternating positions within the arm (Figure 5.3); this is done to achieve a trade-off between performance and manufacturing time. A total of 8 supports was used, placed at regular intervals (40 mm) along the arm (Figure 5.4), to ensure a sufficient number of supports for precise routing, without excessive stiffening of the arm. The diameter of the supports decreases along the arm, always leaving 1 mm of space between it and the mould.

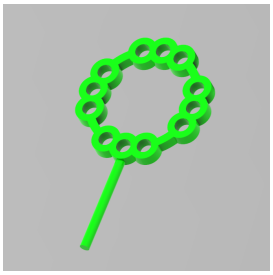

Figure 5.1: Internal support type 1.

Figure 5.2: Internal support type 2.

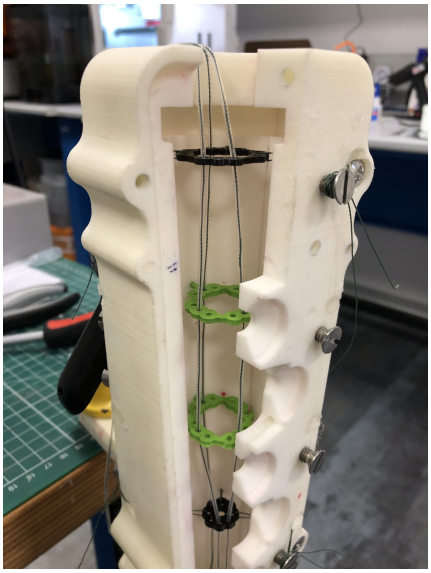

Figure 5.3: The mould during insertion of the internal supports; type 1 supports are shown in green and type 2 supports in black.

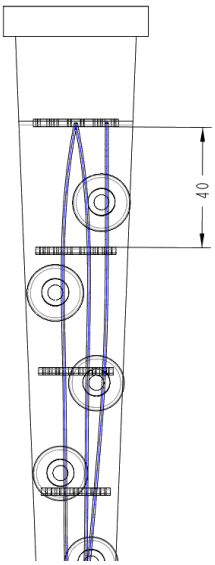

Figure 5.4: Schematic diagram of support distribution; their distance is highlighted once.

For this work, two cable configurations were designed and tested. The selection of these specific routings was driven by the necessity to investigate the influence of the tendon termination point on the arm's curvature profile and active length.

The configurations are:

- **Tendon configuration A** (Figure 5.5a): it consists of a cable for ventral bending anchored to the last support (number 8), a cable for dorsal bending anchored to the penultimate support (number 7), a cable for twisting performing a 180-degree turn, anchored to support number 6.
- **Tendon configuration B** (Figure 5.5b): it consists of a cable for ventral bending anchored to the penultimate support (number 7), a cable for dorsal bending anchored to the last support (number 8), a cable for twisting performing a 180-degree turn, anchored to support number 6.

The bending cables follow a straight path, passing inside the eyelets of all the supports; this allows to obtain bending in the ventral direction (first row of Table 5.1) and bending in the dorsal direction (second row of Table 5.1). The difference between these two configurations lies in the anchoring point of the two cables used for bending, which are swapped in the two configurations; these two configurations were tested and the results are reported below (Table 5.1 and Table 5.2).

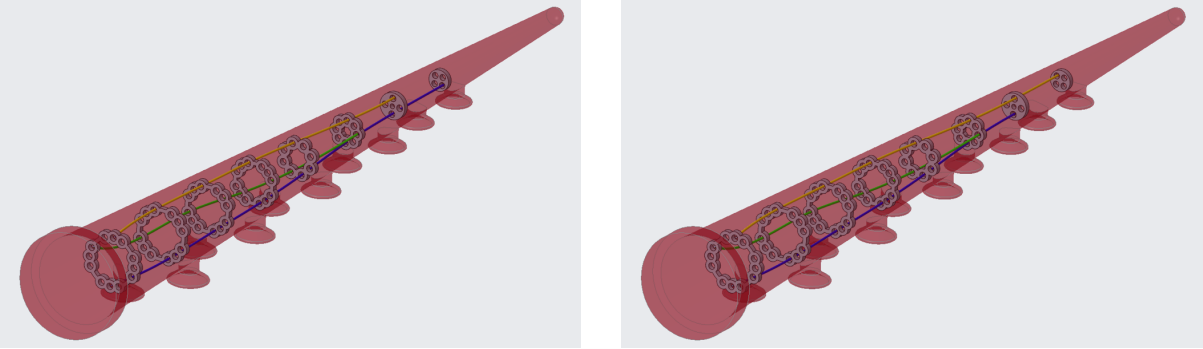

(a) (b)

Figure 5.5: The two tendon configurations designed and tested, configuration (a) on the left and configuration (b) on the right. The cable for ventral bending is shown in blue, the cable for dorsal bending in yellow, and the cable for twisting in green.

The fabrication process consists of the following steps:

- **Mould preparation:** insertion and fixation of internal supports.
- **Tendon preparation:** silicone pipes having inner and outer diameters equal to 1.02 mm and 2.16 mm, respectively, are used to cover the tendon wire and prevent the wearing and tearing of the soft matrix due to friction during regular use.

- **Tendon routing:** the cables are passed through the support eyelets and anchored at the pre-established points.
- **Silicone preparation:** mixing parts A and B of the Ecoflex 00-30 silicone in a 1:1 ratio, insertion of dye (1% red colorant, Silc Pig™ red, Smooth-On Inc.), mixing and defoaming, removal of trapped bubbles thanks to a vacuum chamber.
- **Casting and curing:** pouring the silicone inside the mould and curing (4 hours).

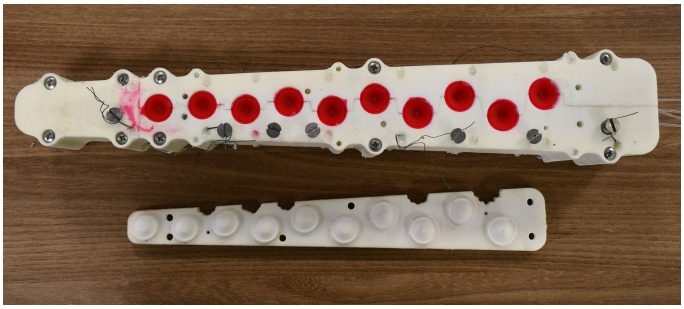

Figure 5.6: The mould after completing all the steps.

5.2. Experimental Characterization

To analyze the obtained movements, tests were performed on tendon configurations A and B. The three cables were actuated one at a time, pulling them by a variable amount between $0cm$ and $11.8cm$, using a system composed of a servo motor and a pulley, that will be analyzed in Chapter 6.

The characterization consisted of measuring the position of a significant point on the arm (different for the 3 movements), varying the amount of cable pulled:

- **Ventral bending and Dorsal bending:** the significant point is the point at maximum distance from the arm axis in the rest position; this is the furthest point where the arm can enter in contact with an object.
- **Twisting:** the significant point is the point lying on the axis of the spiral generated, and placed halfway between the base and the tip of the arm, in the current position; this is the ideal point for an object to enter in contact with the arm, so that it is wrapped by the arm uniformly.

The frames extracted from the tests are reported below:

Tendon Configuration A

	0 cm	5.9 cm	11.8 cm
Ventral Bending	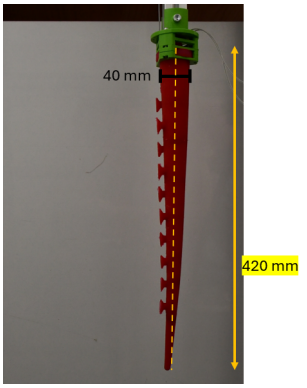	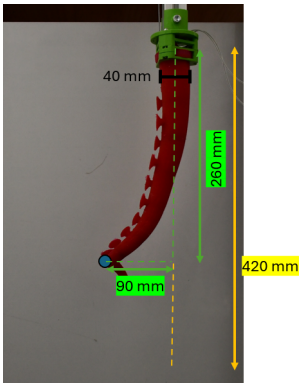	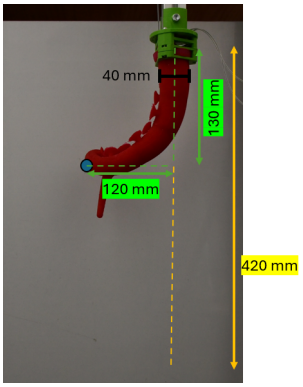
Dorsal Bending	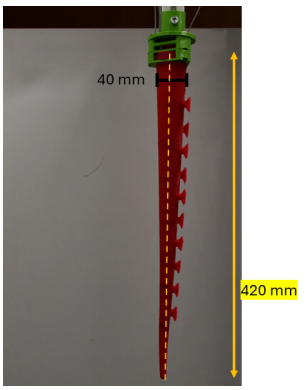	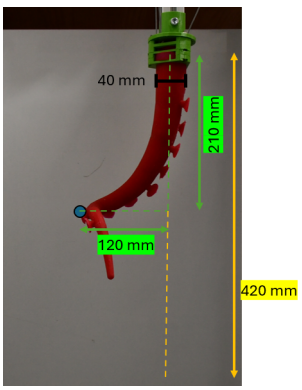	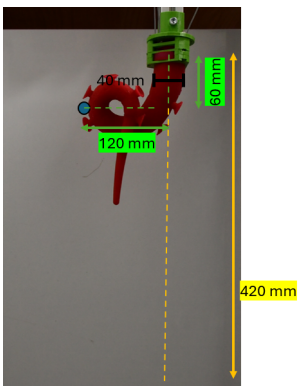
Twisting	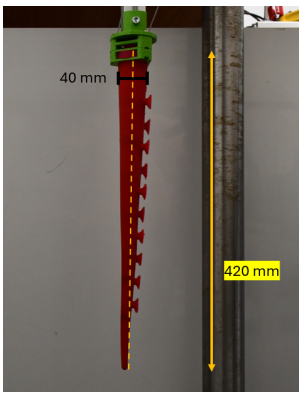	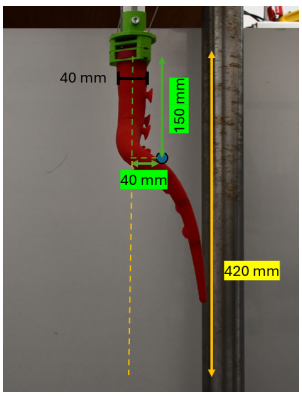	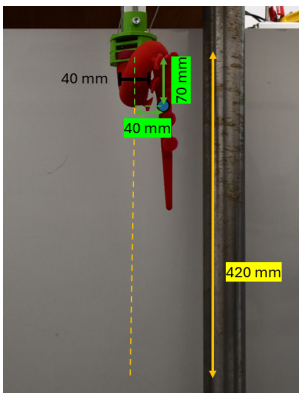

Table 5.1: Experimental characterization of *Tendon Configuration A*. The rows illustrate the three actuation modes (ventral bending, dorsal bending, and twisting), while the columns correspond to tendon displacements of $0cm$, $5.9cm$, and $11.8cm$. The yellow dashed lines represent the axis of the arm in rest position. The points highlighted in blue represent the significant points.

The experimental results for *Tendon Configuration A* demonstrate the high deformability of the soft structure and its ability to achieve the desired kinematic behaviours. The arm starts from an undeformed shape (first column of Table 5.1) and are bent by the actuation of the cables (second and third column of Table 5.2).

Regarding the bending motions (ventral and dorsal), the arm exhibits a continuous curvature along its entire length. As the cable tension increases (from $5.9cm$ to $11.8cm$), the tip of the arm undergoes a significant displacement from the vertical axis (with a maximum of $120mm$). These movements are fundamental to move the arm towards the object (ventral bending), or to spread the arm outwards to create sufficient clearance for object insertion before the grasping (dorsal bending). The effect of the anchoring point can be noted by looking at the shape of the dorsal and ventral bendings: the tendon dedicated to the dorsal bending is anchored at the penultimate support, so it leaves the final segment of the arm partially passive during actuation; the tendon for ventral bending instead is anchored to the last support, applying in this way a force in a point that is further away from the base of the arm, activating almost the entire length of the arm.

Regarding the twisting motion, by pulling the twisting cable it forces the arm to buckle out of the plane, generating a spiral shape. At $11.8cm$ of cable displacement, the arm forms a complete loop. The generated spiral creates a hollow space capable of wrapping around cylindrical or irregular objects. The points highlighted in the frames represent the ideal position of the object to be grasped; by touching the object when it is located at this coordinate, the arm can wrap around it uniformly, maximizing the contact area and, consequently, the friction required to hold the object without active suction.

Also configuration B was tested, to characterize its movements and compare them with the other configuration.

The frames extracted from the tests are reported below:

Tendon Configuration B

	0 cm	5.9 cm	11.8 cm
Ventral Bending	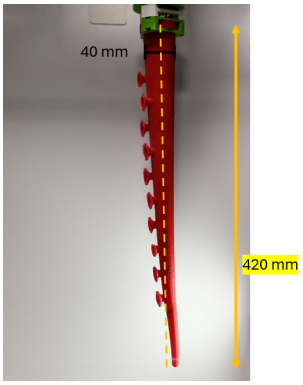	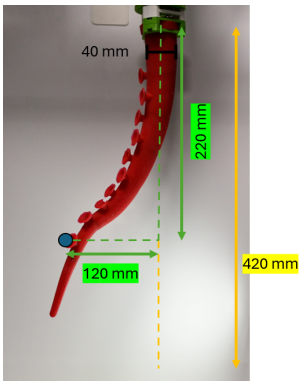	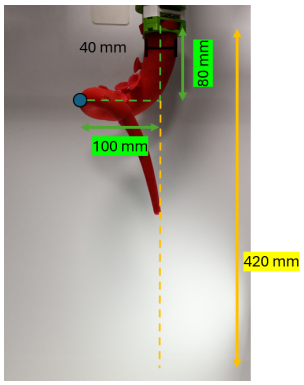
Dorsal Bending	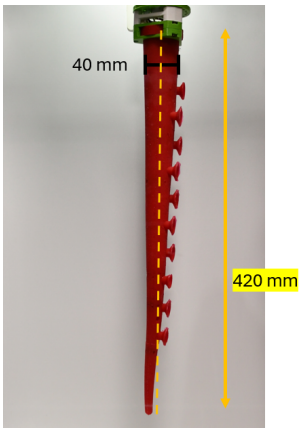	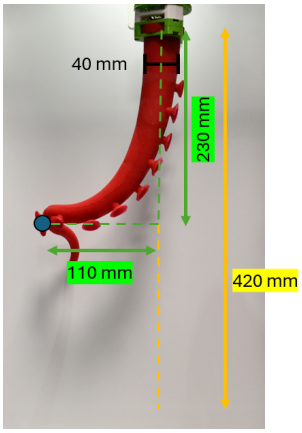	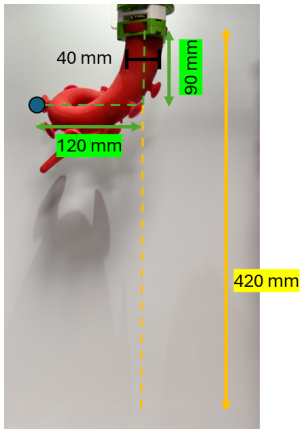
Twisting	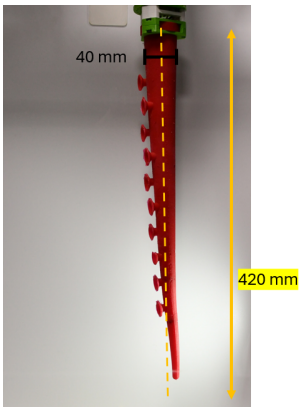	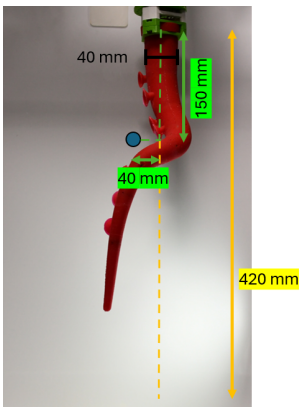	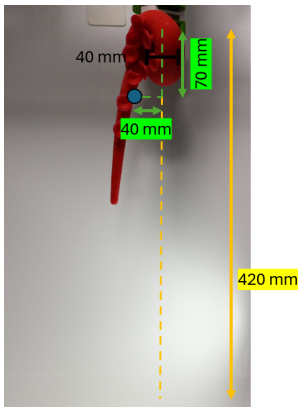

Table 5.2: Experimental characterization of *Tendon Configuration B*. The rows illustrate the three actuation modes (ventral bending, dorsal bending, and twisting), while the columns correspond to tendon displacements of $0cm$, $5.9cm$, and $11.8cm$. The yellow dashed lines represent the axis of the arm in rest position. The points highlighted in blue represent the significant points.

As expected, the twisting motion is identical for configuration A and configuration B, being the cables dedicated to this movement routed in the same way.

Bending movements, instead, show considerable differences. By comparing the ventral bending of the two configurations (Figure 5.7a and Figure 5.7b below), we can see that the bending generated by configuration A is concentrated in the final part of the arm (the significant point is at a distance of 260mm from the base when the cable is pulled by 5.9cm, unlike configuration B, in which the significant point is at a distance of 220mm); this generates a "flatter" profile up to that point, for configuration A. One possible explanation for this flatter profile is that, being anchored to the last support, the tendon dedicated to ventral bending in configuration A has to compress more material in order to make the arm perform the bending movement.
Furthermore, a perfect match was expected for ventral A - dorsal B and for dorsal B - ventral A, having these couples the same routings, but the test did not produce these results: the displacement of the significative point of ventral A (90mm at 260mm from the base, with a 5.9cm cable pulling, and 120mm at 130mm from the base, with a 11.8cm cable pulling) is different from the one of dorsal B (110mm at 230mm from the base, with a 5.9cm cable pulling, and 120mm at 90mm from the base, with a 11.8cm cable pulling). Although these results are not entirely different, the observed differences are significant enough to suggest that the presence of the suckers on the ventral side, plays a role in the deformation profile of the arm during actuation.
The same applies to ventral B - dorsal A couple.

(a) The two ventral bendings with 5.9 cm of cable pulling.

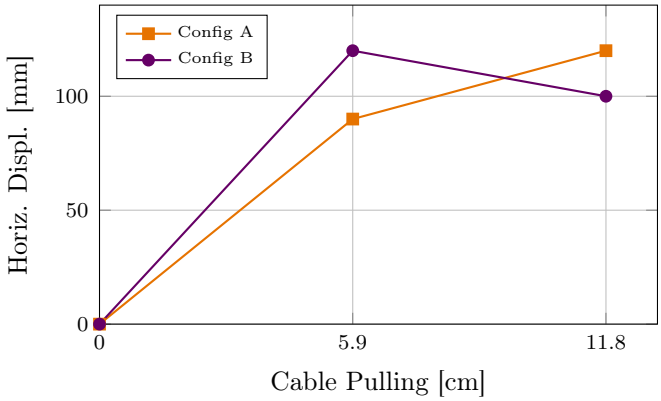

(b) Significative point displacement.

Figure 5.7: Figure 5.7a is a comparison between the ventral bending of configuration A, and configuration B (in transparency). Figure 5.7b shows the horizontal displacement of the significative points (highlighted in 5.7a), as a function of the cable pulling.

These tests are fundamental for obtaining a preliminary idea of arm movements, and the types of grasping that will be possible to perform, but also for making choices about the design of the complete robot:

- With the ventral bending of configuration A, it is expected that grasping will be performed with the entire length of the arm, thanks to the shape assumed by the arm during the intermediate pulling phases; therefore, the arms intended for *pinching* will be chosen with this tendon configuration.
- With the ventral bending of configuration B, it is expected that contact with the object will happen soon, in order to stabilize it; this arm will then be positioned at 90° with respect to the others.
- The "lateral" displacement allows to understand the distance to be maintained between the arms in the robot design, in order to achieve the most complete workspace possible in the volume between the arms, ensuring possible grasping in all this volume; the quantity that emerged from the tests is $12cm$ (Table 5.1, Table 5.2).

These choices will be detailed in Chapter 6.

6 | Multi-Arm Octopus Robot

After fabricating and testing the individual arms, the design and the assembly of the *Multi-Arm Octopus Robot* were addressed. The objective is to evolve the concept of an octopus-inspired robotic gripper from a single arm to a multi-arm system. Such a transition is motivated by the need to explore cooperative manipulation strategies, enhanced grasping capabilities, and more complex interaction scenarios that cannot be addressed with a single manipulator.

The adoption of a multi-arm architecture is justified by several key advantages, that will be investigated:

- **Payload and Geometry:** It enables the manipulation of larger, heavier objects and the robust adaptation to more complex geometries.
- **Dynamic Stability (Caging):** While a single arm might displace a floating object due to fluid interactions, multiple arms can perform caging, enclosing the target from different directions to prevent it from escaping.
- **Bio-inspiration:** This evolution better mimics the biological model, where the octopus dynamically recruits multiple arms to maximize stability and adhesion during grasping tasks (Chapter 4).

The initial design phase consisted of setting the following design variables:

- The number of arms.
- The relative position between the arms, their orientation, and their relative movements.
- The deformation movements allowed for each arm.

Regarding the choice of the number of arms, the data collected during the experiments in *Acquario di Genova*, described in Chapter 4, were used: the number of arms used simultaneously for object manipulation was statistically observed to be 2/3 (Figure 4.10). The options were therefore to use 2 arms or 3 arms in the design. However, aiming at replicating the new grasping strategies discovered in this work (Section 4.3), the 2-arm

option was discharged, as it would have made impossible to replicate the *Basal grasping* movement, which uses 3 arms.

The choice of the relative position between the arms, their orientation, and their relative movements was also guided by these results, as will be explained in Section 6.1.

The deformation movements allowed for each individual arm are those designed and tested during the single arm design phase (Chapter 5), with the two types of tendon configurations (A and B); therefore, will be present 3 ventral bendings, 3 dorsal bendings, and 3 twistings.

It is important to clarify the scope of the proposed design: the platform is not intended as a final, fully waterproofed solution for deep-sea exploration. Instead, it represents a preliminary study platform aimed at validating the transition from single-arm to multi-arm architectures. This setup allows for the assessment of new arms-object interactions, cooperative workspace, and control algorithms before moving towards a more compact, ROV-ready design.

6.1. Mechanical Design

As anticipated, the robot design started from the results of the experiments conducted in *Acquario di Genova*, following the philosophy of bio-inspired robotics; the relative position between the arms, their orientation, and their relative movements were indeed designed to replicate the two identified movements.
The robot was designed to have two configurations:

- ***Pinching configuration*** (Figure 6.1a): Two arms in the frontal section, with the ventral side facing each other, capable of moving translationally one towards the other; one arm in the rear section, with the ventral side facing the frontal section. With this configuration, it is expected to grasp objects located on the sliding axis of the two frontal arms, using the full length of these arms, as well as the third arm (the rear one), thanks to the use of its ventral bending / twisting.
- ***Basal Grasping configuration*** (Figure 6.1b): Two arms in the frontal section, with the ventral side facing the rear section, capable of moving translationally one towards the other; one arm in the rear section, with the ventral side facing the frontal section. With this configuration, it is expected to grasp objects whose axis is oriented horizontally, using the ventral bending of all the three arms.

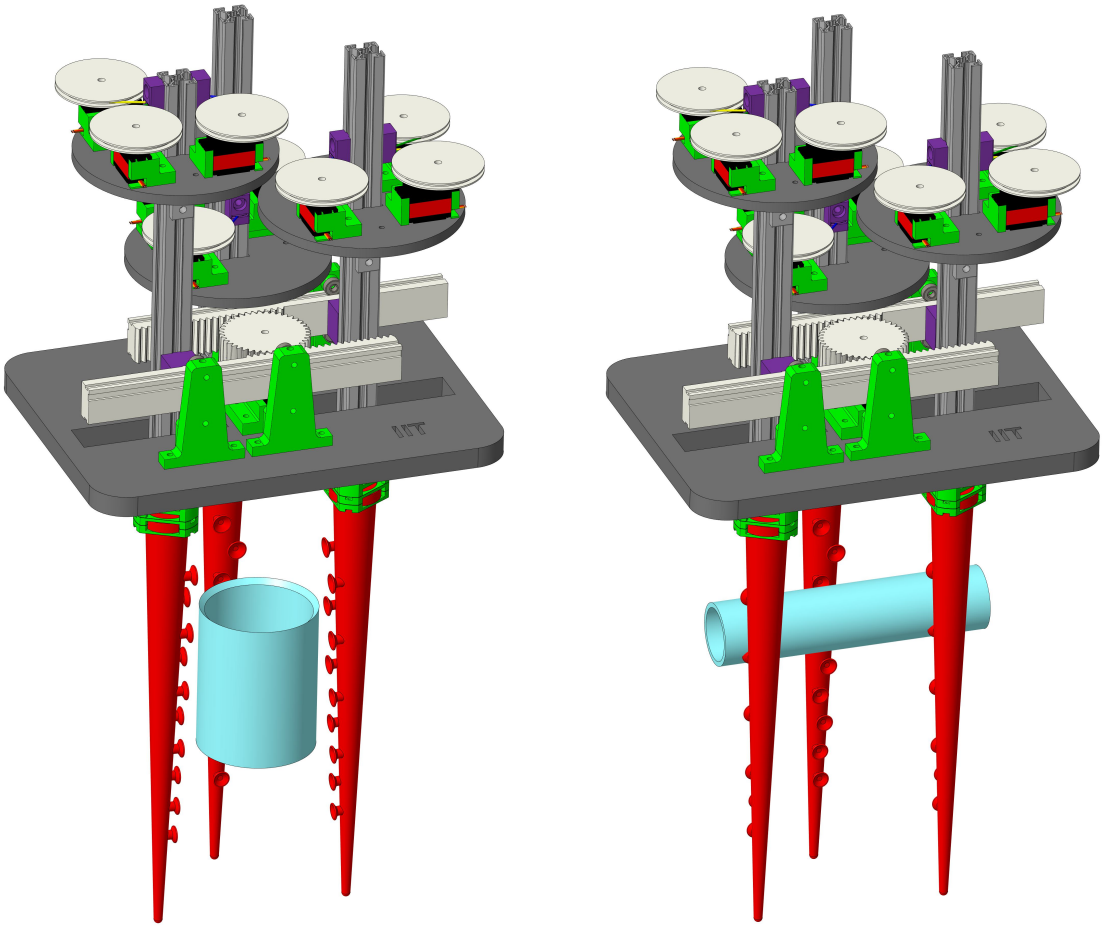

(a) (b)

Figure 6.1: CAD model of the Multi-Arm Octopus Robot mounted in *pinching configuration* (a) or *Basal grasping configuration* (b).

To switch from one configuration to the other, human intervention on the arms is required, rotating the two frontal arms by 90°, with a rapid but non-automatic procedure. These two configurations will be tested separately (Chapter 7).

Based on the tests performed on the single arms, it was decided to use the following combination of tendon configurations:

- Frontal arms = Tendon configuration A
- Rear arm = Tendon configuration B

These choices derive from the shape that the two configurations assume during ventral grasping: for the frontal arms, used for pinching, less pronounced bending is required, distributed more uniformly along the entire length of the arms (Section 5.2); for the rear

arm, configuration B was chosen due to its pronounced ventral bending (Section 5.2), which is expected to establish the contact with the object from greater distances during *pinching*, and wrapping the object during *basal grasping*.

The mechanical design is composed of:

- **Support Base** (Figure 6.2): The structural frame, necessary for fixing the robot (to the ground or on an ROV, in the future), and for positioning the 3 arms (2 movable with a rack-and-pinion translational mechanism and 1 fixed).
- **Tendon Actuation Units** (Figure 6.6): 3 circular bases, placed in the upper part, housing the motors and their additional components (pulleys and cable deflection guides).
- **Electronic Architecture**

Below, all design components will be analyzed, with a focus on their geometry, functionality, and integration into the system.

Support Base

It consists of a rectangular platform (gray in Figure 6.2), laser-cut from a sheet of POM (Polyoxymethylene); it features rectangular slots, designed to accommodate the aluminum profiles supporting the arms. This base allows to be placed and fixed, ensuring stability to all robot components (in this case, for testing, it was fixed on aluminum profiles on top of an aquarium (Figure 6.3).

Fundamental components are placed on this base: to realize the additional translational DOF, a rack-and-pinion mechanism was designed (white in Figure 6.2). A central pinion (3D printed in PLA), driven by a dedicated servo motor, transfers its motion to 2 racks (3D printed in PLA), transforming rotational motion into linear motion. The two arms are rigidly fixed to these two racks, keeping both centered on the translational axis, thanks to two spacers (purple in Figure 6.2). For the positioning of the rack-and-pinion mechanism, the presence of 4 "bearing blocks" on the rectangular base is necessary (green in Figure 6.2), upon which 3 ball bearings each are mounted; these bearings roll along guides embedded in the racks, allowing precise centering, without clearance, and efficient sliding, with low energy dissipation. The two bearing blocks of each rack are spaced, to be able to support the moment generated by the weight of the arms, which is absorbed by the bearings.

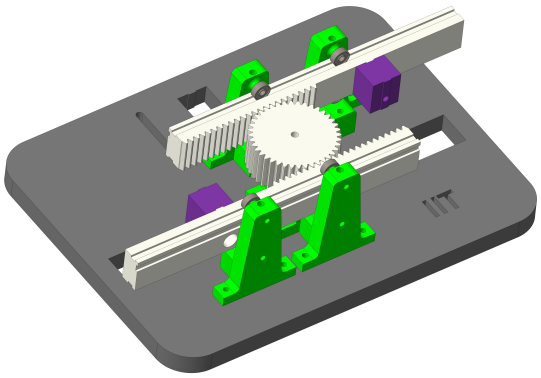

Figure 6.2: CAD model of the support base. The rack-and-pinion, the bearing blocks and the spacers are highlighted.

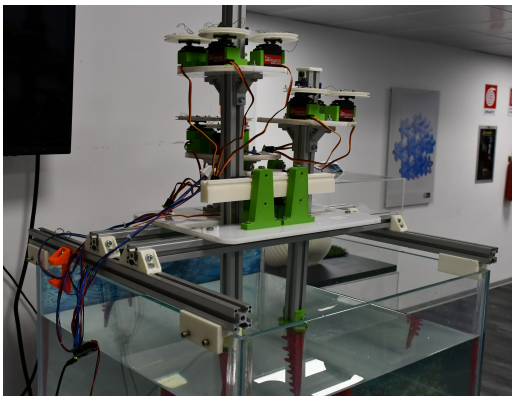

Figure 6.3: Robot mounting setup. It is fixed on aluminum profiles on top of the aquarium.

The pitch diameter of the pinion (D_p) was selected as follows: taking into account the design constraint of the rotation limit of the servo motors used ($\Delta\theta_{\max} = 180° = \pi$ rad) (the technical characteristics will be described later), the size of the pinion diameter necessarily had to be a trade-off between the stroke (S) of the translational mechanism (the smaller the diameter, the shorter the stroke, with a relationship expressed by Equation 6.1) and the minimum distance between the arms when the motor reaches the limit rotation (the smaller the diameter, the smaller this distance).

$$S = \Delta\theta_{\max} \cdot \frac{D_p}{2} = \pi \cdot \frac{D_p}{2} \tag{6.1}$$

Both these aspects are important for effective pinching: if the stroke is too short, the arms cannot expand/converge sufficiently to approach/compress an object; if the minimum distance between the arms is too large, grasping small objects becomes impossible.

The specifications of the pinion are listed in Table 6.1.

Symbol	Description	Value	Unit
m	Gear Module	2	mm
z	Number of Teeth	40	-
α	Pressure Angle	25	°
D_p	**Pitch Diameter** $(m \cdot z)$	**80**	**mm**

Table 6.1: Geometric parameters of the pinion.

The chosen pitch diameter ($D_p = 80mm$) allows for a stroke $S = 12.5cm$ (using Equation 6.1), with a minimum distance between the arms $s_{\min} = 12cm$ (pinion diameter + aluminum profile width) and therefore a maximum distance between the arms $s_{\max} = 37cm$ (Equation 6.2).

This minimum distance is ideal because, as seen in Section 5.2, the frontal arms have a ventral bending with which they can reach a distance of $12cm$ from the axis of the arm in resting position, thus enabling contact with objects using always at least two arms in the entire volume enclosed by the arms. The maximum distance is sufficient to wrap around very large objects; moreover, this dimension can be further increased by exploiting the dorsal bending of the arms.

$$s_{\max} = s_{\min} + 2 \cdot S \tag{6.2}$$

The distance of the third arm from the translational axis of the two frontal arms was left manually adjustable, using a screw-and-slot mechanism (in the upper part of Figure 6.2), to enable testing in different positions; its default position is $12cm$ from this axis, to achieve a symmetric triangular configuration when the arms are at minimum distance (Figure 6.4).

The arms are fixed to the ends of the aluminum profiles with a locking system (Figure 6.5) composed of 3 pieces (3D printed in PLA), which allow for:

- Solid fixation, without compressing the internal tendons.
- Possibility of rapid manual adjustment to switch from the *pinching* configuration to the *basal grasping* configuration, by rotating the arm.
- Passage of the tendons, which continue in a straight line towards the Tendon Actuation Units.

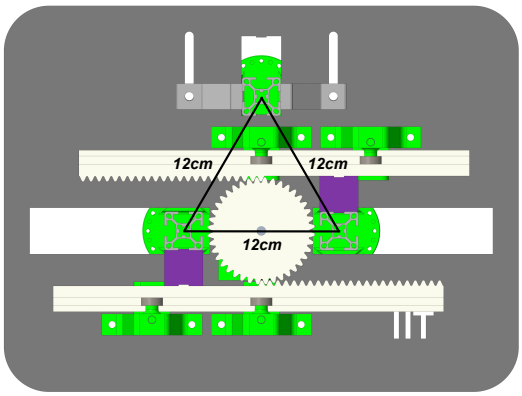

Figure 6.4: Top view of the arms in minimum distance position.

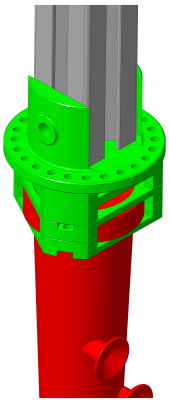

Figure 6.5: Locking system of the arms.

Tendon Actuation Units

These 3 platforms, one for each arm, are fundamental for arm actuation. They are positioned above the Support Base and consist of a circular base (grey in Figure 6.6), laser-cut from a sheet of POM; they feature a rectangular slot through which passes the aluminum profile supporting the arm.

On top of each of them, 3 Amewi 6221MG servo motors are fixed (technical specifications listed in Table 6.2), each one pulling a cable with a pulley (white in Figure 6.6). The dimensioning of the pulley diameter (D_{pulley}) was driven by the required tendon excursions; specifically, these arms reach their maximum designed bending when the tendon is pulled of $11.8cm$. So, given the fixed rotation range of the servo motor ($\Delta\theta_{\max} = 180° = \pi$ rad), and the relationship between the tendon displacement (ΔL) and the pulley rotation (Equation 6.3), the pulley diameter was selected to be $D_{\text{pulley}} = 7.5cm$.

$$\Delta L = \frac{D_{\text{pulley}}}{2} \cdot \Delta\theta_{\max} = 11.8cm \tag{6.3}$$

These motors were selected for their high torque (verified to be sufficient to pull the tendons, thanks to the tests performed with a universal testing machine in Chapter 7), for their sufficient movement speed (higher speeds are not required for underwater grippers, because of the high drag in water), and for their low cost.

The last elements present in the Tendon Actuation Units are the cable deflection guides (purple in Figure 6.6): these are necessary to transform the vertical movement of the tendons into an horizontal movement, enabling their winding and securing on the pulleys.

Parameter	Value	Unit
Motor Type	Digital	-
Gear Material	Aluminium	-
Operating Voltage	4.8 – 6.0	V
Stall Torque (6V)	20.32	kg·cm
Operating Speed (6V)	0.16	sec/60°
Dimensions	40.5 × 20.2 × 38	mm
Weight	62	g

Table 6.2: Technical specifications of the Amewi 6221MG Servo Motor.

These elements were designed to allow smooth sliding of the tendons on their surface, without the risk of tendon wearing.

The weight of the entire system (Support Base + three Tendon Actuation Units) is 8 kg. This is considered suitable for the current developmental stage, allowing for easy manual transportation. It should be noted that the current structure was designed with a focus on stiffness and modularity; therefore, mass reduction strategies can be easily applied in future developments, to significantly lower the total weight.

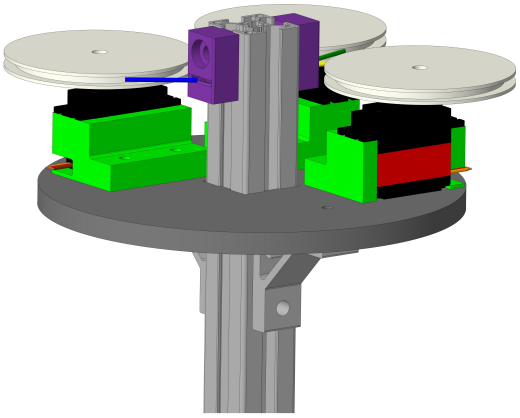

Figure 6.6: CAD model of a tendon actuation unit.

Electronic Architecture

The electronic system was designed to ensure precise signal generation for the multiple actuators and stable power distribution, minimizing the risk of voltage drops during high-load operations. The architecture is centered around a single microcontroller unit and a bench power supply (Figure 6.7).

The core control unit is an *Arduino Nano 33 IoT*; this microcontroller was selected for its compact form and its sufficient number of PWM-enabled Digital I/O pins, which are necessary to independently control all the servo motors (3 for each arm, plus the rack-and-pinion actuation motor). Power is supplied to the motors by an external regulated bench power supply, set to a constant voltage of 6V to match the optimal operating range of the actuators.

To simplify the cabling layout, small connection boards were used on each unit. Each of the three *Tendon Actuation Units* is equipped with a custom *signal distribution board*, that acts as a connection hub, where the cables are soldered and organized. The wiring scheme is organized as follows:

- The power lines (+6V and GND) and the specific PWM signal lines from the Arduino are routed to these local boards.
- From each board, the lines are directed to the three servo motors housed in that specific unit.

This setup ensures that the current flow required by the servomotors during the grasping phases does not affect the microcontroller logic.

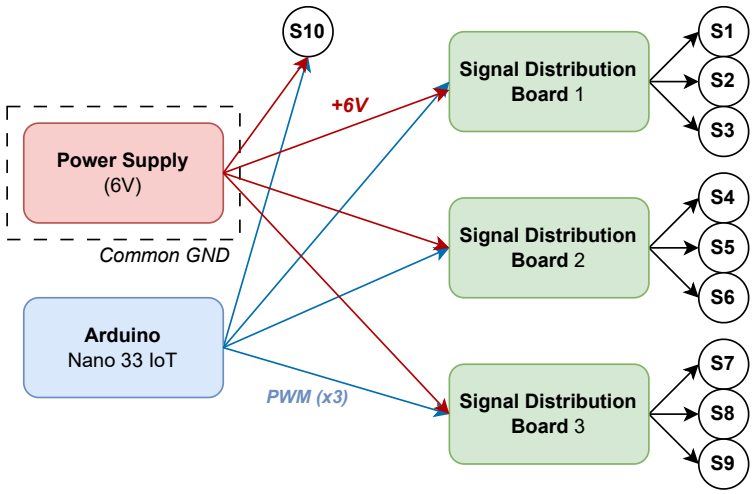

Figure 6.7: Schematic representation of the electronic architecture. The diagram illustrates the central control unit (Arduino Nano 33 IoT), the external power supply, and the custom signal distribution boards located on each Tendon Actuation Unit to manage the connections for the 9 servo motors of the arms; the servo motor number 10 is the one dedicated to the rack-and-pinion mechanism.

6.2. Control Strategies

The control architecture of the *Multi-Arm Octopus Robot* is designated to manage the actuation of an high number of degrees of freedom (DOF) simultaneously, while ensuring smooth motion and requiring simple inputs from the user.

To address this, a custom control strategy was developed, focusing on three key aspects:

1. **Parallelism (Non-blocking):** Simultaneous control of 10 independent degrees of freedom (9 for the arms, 1 for the rack-pinion mechanism) using a single microcontroller.
2. **Position Control with Velocity Profiling:** Given the soft nature of the robotic arms and the tendon-driven mechanism, standard step-response control, where the servo moves to the target position at maximum speed, is unsuitable; it would cause undesirable oscillations and high mechanical stress on the tendons.
3. **Simplified Command Interface:** The control hides the complexity of the motion generation. This allows the user to simply send target positions of the motors, while the Arduino automatically handles the speed profile and timing.

The developed code, running on the Arduino Nano 33 IoT, abandons the standard blocking "delay()" functions, using instead a non-blocking scheduling approach, based on the system timer. In a standard blocking approach, the processor waits for a motor to complete its movement before processing the next instruction. This would result in a sequential movement of the motors, not suitable to achieve the desired grasping movements. Here instead, the code cyclically checks the state of all 10 motors, and if a specific time interval Δt (related to the desired speed) has passed since the last update, the motor position is incremented or decremented by a single step towards the target. This allows the robot to update the trajectories of all actuators simultaneously, while remaining responsive to incoming serial commands.

The logical flow of this control strategy is formalized in Algorithm 6.1.

By selecting the Δt parameter, is therefore possible to set a suitable speed for the actuation, solving the problem of oscillations and undesired stress on the tendons: the larger this parameter is, the slower the movement speed will be, as position updates will be made at longer intervals.

The communication with the user is established through a serial protocol. The command syntax follows the structure:

```
[Motor ID]  [Target Angle]
```
(6.4)

For example, sending the string "`2 180`" moves the motor number 2 to 180°. This concept also applies to the simultaneous movement of multiple motors (for example, sending the string "`2 180 9 45`" moves the motor number 2 to 180° and the motor number 9 to 45°). Additionally, a `RESET` command ("r") was implemented to instantly recall all actuators to their "home position", facilitating rapid testing cycles.

The algorithm begins with an **Initialization Phase (Lines 1-5)**, where the 10 motors are moved to the calibrated $Home\_Pos$, and the $Current\_Pos$ array is updated. Crucially, the $Last\_Update$ array is populated with the current system time; this array acts as the time reference for each motor. Here is also set the Δt parameter.
Inside the main loop, the operations are split into two distinct blocks:

1. **Command Parsing Phase (Lines 7-16):** This block listens for user input on the serial port: when a standard command is received, the code updates the specific values in the $Target\_Pos$ array; when the `RESET` command is received, it triggers an update of the entire $Target\_Pos$ array, setting it to $Home\_Pos$. This update is still governed by the logic of the Actuation Phase, ensuring that even the system reset is performed with controlled velocity.

2. **Actuation Phase (Lines 17-30):** This is the core of the control strategy. The code iterates through all the 10 motors in every cycle: for each motor i, the algorithm checks if a specific time interval Δt has elapsed since the last movement.

    - If the condition is met, the $Last\_Update$ time vector is updated, and the motor performs a single incremental step ($+1$ or -1) to reduce the gap between $Current\_Pos[i]$ and $Target\_Pos[i]$.

    - If the condition is not met, the motor remains in its state, and the loop proceeds to the next motor.

This architecture allows the predefined key aspects to be met, ensuring simultaneous movement, speed control, and simple user input requests. To further enhance the user experience, future developments could integrate a Graphical User Interface (GUI), providing a more intuitive visual control panel.

Algorithm 6.1 Non-Blocking Control Loop

Require: System Initialization, calibrated $Home\_Pos$

Initialize all Motors to $Home\_Pos$
$Target\_Pos[1..10] \leftarrow Home\_Pos$
$Current\_Pos[1..10] \leftarrow Home\_Pos$
$Last\_Update[1..10] \leftarrow$ millis()
$\Delta t \leftarrow$ SpeedDelay
while System is Running **do**
  // 1. Command Parsing Phase
  if Serial Data Available **then**
    Read Command
    if Command is RESET **then**
      $Target\_Pos \leftarrow Home\_Pos$
    else
      $Motor\_ID,\ New\_Angle \leftarrow$ **Parse**$(Command)$
      $Target\_Pos[Motor\_ID] \leftarrow New\_Angle$
    end if
  end if
  // 2. Actuation Phase (Parallelism)
  for $i \leftarrow 1$ **to** 10 **do**
    $Time_{now} \leftarrow$ millis()
    if $(Time_{now} - Last\_Update[i]) > \Delta t$ **then**
      $Last\_Update[i] \leftarrow Time_{now}$
      if $Current\_Pos[i] < Target\_Pos[i]$ **then**
        $Current\_Pos[i] \leftarrow Current\_Pos[i] + 1$
        ServoWrite$(Motor_i,\ Current\_Pos[i])$
      else if $Current\_Pos[i] > Target\_Pos[i]$ **then**
        $Current\_Pos[i] \leftarrow Current\_Pos[i] - 1$
        ServoWrite$(Motor_i,\ Current\_Pos[i])$
      end if
    end if
  end for
end while

It is worth noting that, although the non-blocking algorithm technically enables the simultaneous actuation of all 10 degrees of freedom, a fully synchronous activation of the entire system is not required for effective grasping tasks. Furthermore, the simultaneous high-torque actuation of all motors could lead to significant peak current absorption, potentially stressing the power supply unit.

Consequently, to ensure electrical stability and to replicate the coordinated movements observed in the biological model, a set of predetermined movements was defined and tested, as will be described in the next chapter.

7 | Experimental Validation and Results

An extensive experimental campaign was conducted to evaluate the performance of the *Multi-Arm Octopus Robot*. The objective of this chapter is to validate the engineering choices described in Chapter 6, and to assess the robot's capability to replicate the biological grasping strategies analyzed in Chapter 4. The validation process is organized into two main sections: first, the experimental framework is defined, analyzing the testing environment, the set of movements used, and the kinematic workspace of the robot; second, the grasping performance is quantitatively assessed through tests in both air and water, followed by a discussion on the energy efficiency of the adopted grasping strategies.

7.1. Framework and Workspace

The experiments were conducted in a controlled environment designed to simulate static underwater conditions. The robot is mounted above a 60x60x60cm tank, with the arms completely submerged in water, up to the base (Figure 7.1). The videos were recorded with a Nikon D7500 camera, and significant frames were extracted, to clearly illustrate the movements of the arms and the grasping sequence.

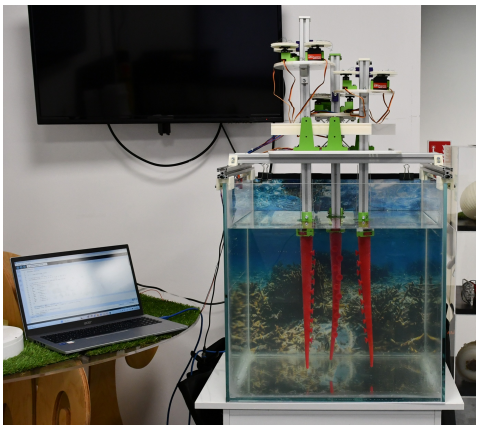

Figure 7.1: Experimental setup.

As first step, the proper functionality of the rack-and-pinion translational mechanism was validated, confirming its effectiveness in smoothly adjusting the distance between the frontal arms. To perform the discovered *Pinching* and *Basal Grasping* strategies, after a preliminary refinement phase, this sequence of control actions was adopted:

1. **Approach:** Simultaneous actuation of the translational DOF (extended to its maximum stroke of $37cm$), and of the three dorsal cables (pulled to 100% of their maximum displacement of $11.8cm$). This is needed to provide sufficient clearance for the approach to the target object.
2. **Pre-Grasp Shaping:** Calibration of the distance between the frontal arms, actuating the translational DOF; three distances for each object were tested, as will be explained in Section 7.2. During this motion, a relaxation of the dorsal cables is also applied, to recover the initial straight position of the arms.
3. **Grasping Execution:** Simultaneous actuation of the three ventral cables; two different tendon actuation percentages were tested (50% and 80%), as will be explained in Section 7.2.

Clearly, these control actions are performed with the *Pinching* and *Basal Grasping* relative configurations of the arms (Figure 6.1). Points 2 and 3 are replaced by a combination of twisting and bending cable pulling, in the case of alternative grasping attempts (Figure 7.13). To visualize the operational volume covered by the three arms in water during these phases, a motion envelope was generated by extracting and superimposing significant frames of the arms motion.
During the *Approach* phase, the arms are bent outwards, thus enlarging the space between them (Figure 7.2). The volume covered by the arms is in this case a *reachable space*, since the arms are not capable of grasping an object in this volume, but only of reaching these points, thanks to the actuation of the cables. This space can be further enlarged by using the translational DOF, allowing the approach of objects up to $40cm$ wide.
During the *Grasping Execution* phase, the arms are bent inwards, thus entering in contact with the object in the volume between the arms. The object is assumed to be centered between the frontal arms, aligned with the rear arm, as the grasping sequence naturally guides and compresses it into this region, regardless of its original horizontal position. As the ventral cables are pulled, the arms expand the volume within which they can apply forces to the object's external surface. By applying a 50% tendon actuation, the effective grasping volume is relatively small and localized in the lower part of the arms (green region in Figure 7.3a), conversely, an object fully contained within the upper volume between the arms (yellow region in Figure 7.3a) will experience no applied force. Despite

the high softness of the arms in the lower portion, this configuration still proved to be effective during testing. In this case, the volume is a *functional workspace*, as the arms are able to perform grasping inside it. By applying an 80% tendon actuation, the workspace is stretched upwards (green region in Figure 7.3b). Given the softness of the arms, in these volumes the arms not only come in contact with the object, but also adapt to it; in particular, for objects of the same size, an higher pull (80%) allows both greater compression and more effective modeling around the surface of the object, facilitating also the adhesion of the suckers.

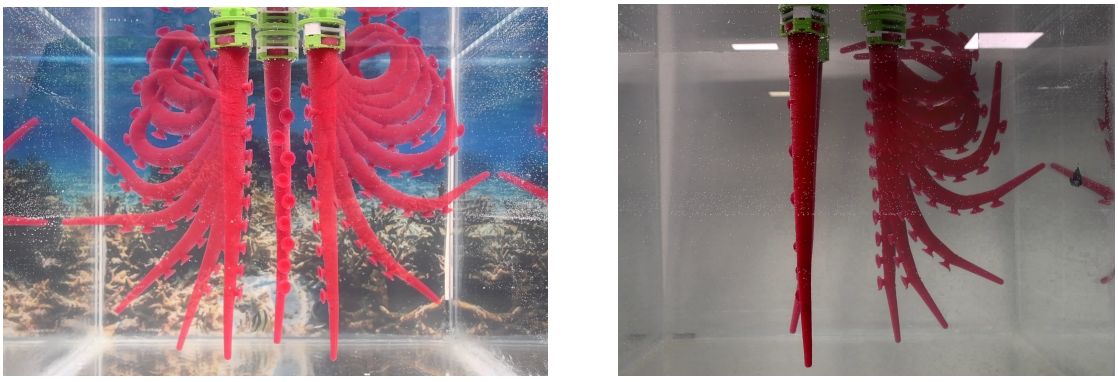

(a) (b)

Figure 7.2: Dorsal bending of the arms during the *Approach* phase. The motion envelope is displayed from (a) frontal and (b) lateral views, to highlight the overall reachable space.

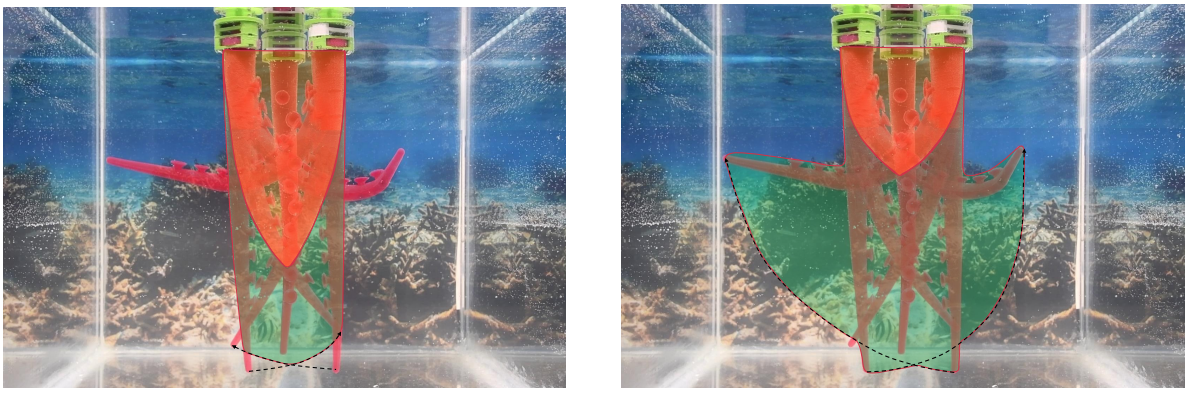

(a) (b)

Figure 7.3: Functional workspace during the *Grasping Execution* phase. With 50% tendon actuation (a) and 80% tendon actuation (b). The movement of the arms (highlighted by the arrows) define the volume in which they can apply a force (green volume). Small asymmetries are caused by the intrinsic softness of the silicones, which are not suitable for very precise positioning of the tips.

To expand this workspace, the translational DOF can be used (Figure 7.4). If twisting is used instead, the arms can be moved out of the bending plane of the frontal arms (Figure 7.5); by combining this movement with ventral bending, it is possible to extend the workspace into the volume located ahead of the frontal arms, and to grasp objects also in this region (Figure 7.13). It can be noted that the twisting motion in water generates a more "lateral" movement compared to the equivalent motion in air, where the arms assume a more pronounced spiral-like shape (Table 5.2).

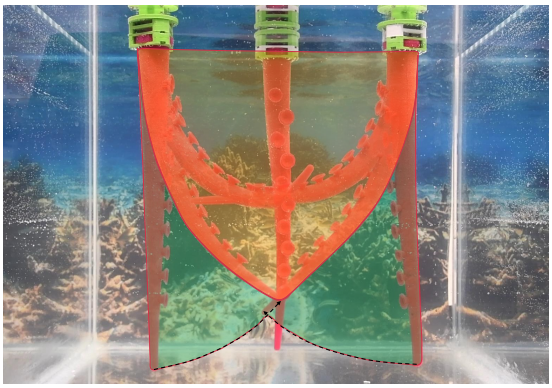

Figure 7.4: Expansion of the functional workspace using the translational DOF, and 50% tendon actuation.

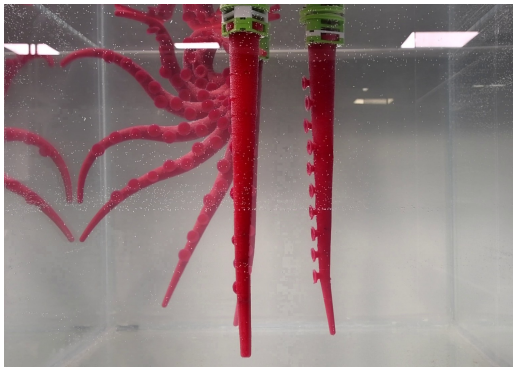

Figure 7.5: Out-of-plane motion generated by twisting, seen from a lateral perspective.

7.2. Grasping Performance

The evaluation of the grasping performance was conducted through a series of dynamic tests, designed to quantify the maximum payload capacity of the multi-arm system under different configurations. To simulate the interaction with delicate organisms, all the target objects selected for the tests are made of light plastic and feature complex, curved geometries (detailed in Figure 7.6). These specific shapes are notoriously challenging for traditional rigid grippers: without a narrow flat surface to be pinched, a rigid mechanism fails to grasp large or round objects (such as the barrel or the spheres), as they tend to slip away unless compressed with perfectly symmetrical forces. At the same time, rigid grippers would irreversibly crush or damage delicate targets. The *Multi-Arm Octopus Robot*, instead, relies on its intrinsic softness to adaptively grasp the objects, exploiting both friction and sucker adhesion.

(a) (b) (c) (d) (e)

Figure 7.6: Set of objects used for the experimental grasping tests: (a) becher, (b) barrel, (c) large sphere, (d) small sphere, and (e) box. For each object, the dimension highlighted in orange represents the characteristic length (L_c), defined as its horizontal width.

The quantitative results are summarized in Table 7.1 for the tests conducted in air, and Table 7.2 for the aquatic environment. The tables are designed to compare the performance of a single arm (*1 ARM* column) with the cooperative manipulation of the novel system (3 ARMS columns), and also to evaluate the effectiveness of its different operational modes. For the three-arm configuration, the *Pinching* strategy was tested across three different translational distances of the frontal arms ($0.75L_c$, $1.0L_c$, and $1.25L_c$, where L_c is the characteristic length of the object, highlighted in Figure 7.6) and two tendon actuation percentages (50% and 80%).
It is important to note that the experimental tests were bounded within specific kinematic and actuation limits. These thresholds were established during a preliminary refinement phase for the following reasons:

- **50% tendon actuation (Lower limit):** Below this threshold, the arms were unable to achieve sufficient stiffness to perform a stable grasp, failing to secure the objects.
- **80% tendon actuation (Upper limit):** Actuating the cables beyond this value, often a "buckling out of the bending plane" occurred (Figure 7.7). Instead of compressing the object further, the arms suddenly twisted sideways, losing contact with the target.
- **$1.25L_c$ translational distance (Upper limit):** Widening the space between the frontal arms beyond this point, resulted in unsuccessful grasping attempts, regardless of the applied tendon actuation percentage.
- **$0.75L_c$ translational distance (Lower limit):** Given the mechanical limitation of $12cm$ as the minimum distance between the arms of the robot, the 0.75 threshold was inevitable for some objects (like the small sphere), while for others the problem

was again the buckling out of the bending plane, as also the translational compression influences this event, especially when combined with high tendon actuation.

The *Basal Grasping* strategy was also evaluated; in this operational mode, all three ventral cables were simultaneously pulled to an 80% actuation level to maximize the wrapping effect around the target.

The following notations are used throughout the tables:

- **X** : Indicates a complete grasping failure. In this condition, the robot is unable to secure the object, even without any extra applied weight.
- **-** : Indicates a configuration that is mechanically unreachable due to geometrical constraints.
- $\boldsymbol{m_1 < m < m_2}$: Represents the payload range, in grams. Below the value m_1, the grasp is stable; at m_1, the object begins to exhibit sliding (at least one slip was recorded during the grasping attempts); at m_2, the grasping fails immediately, and the object drops. It is crucial to report this range because the intrinsic compliance of the silicone often allows the object to slightly slip initially but then re-settle and stabilize in a lower position within the arms.

The payload ranges presented in the tables do not derive from a statistical analysis of success percentages. Rather, they represent the empirical values at which the arms demonstrated a consistent and repeatable grasping capability across multiple attempts.

The two rows related to the barrel (b) represent two different orientations of the barrel itself (the first vertical and the second horizontal), given that its geometry and proportions allowed for separate study. It can be noted that in the single-arm tests (*1 ARM* column) is not present a range, but only a single failure value. This occurs because a single arm lacks the opposing forces provided by the other arms; therefore, once the object slips, it cannot re-settle and it falls immediately.

	1 ARM	3 ARMS						
		PINCHING						BASAL GRASP.
		$0.75L_c$		L_c		$1.25L_c$		
		50%	80%	50%	80%	50%	80%	
a	X	-	-	$128 < m < 178$	$208 < m < 308$	$108 < m < 208$	$208 < m < 258$	$218 < m < 248$
b	X	$306 < m < 326$	$306 < m < 366$	X	$306 < m < 336$	X	$266 < m < 286$	X
	X	$316 < m < 356$	$366 < m < 416$	$266 < m < 296$	$326 < m < 356$	X	$296 < m < 326$	$266 < m < 306$
c	X	$228 < m < 258$	$248 < m < 298$	$208 < m < 248$	$238 < m < 278$	$178 < m < 238$	$198 < m < 228$	X
d	X	-	-	-	-	$48 < m < 68$	$58 < m < 78$	X
e	79	$89 < m < 109$	$109 < m < 129$	$79 < m < 109$	$89 < m < 119$	$79 < m < 99$	$89 < m < 119$	$169 < m < 259$

Table 7.1: Grasping performance results in air.

	1 ARM	3 ARMS						
		PINCHING						BASAL GRASP.
		$0.75L_c$		L_c		$1.25L_c$		
		50%	80%	50%	80%	50%	80%	
a	69	-	-	$225 < m < 283$	$362 < m < 406$	$165 < m < 219$	$258 < m < 305$	$285 < m < 323$
b	30	$412 < m < 431$	$424 < m < 461$	$332 < m < 372$	$402 < m < 441$	X	$342 < m < 382$	X
	118	$396 < m < 453$	$433 < m < 455$	$346 < m < 394$	$406 < m < 453$	X	$366 < m < 402$	$334 < m < 352$
c	98	$295 < m < 344$	$374 < m < 424$	$266 < m < 335$	$319 < m < 378$	$241 < m < 295$	$297 < m < 354$	X
d	30	-	-	-	-	$59 < m < 81$	$63 < m < 93$	X
e	69	$118 < m < 145$	$147 < m < 179$	$106 < m < 145$	$120 < m < 157$	$106 < m < 138$	$118 < m < 167$	$227 < m < 366$

Table 7.2: Grasping performance results in water.

Regarding the performance of 1 arm compared to that of 3 arms, the multi-arm configuration showed a significantly extended payload capacity across the entire tested object set. In air, the single arm successfully grasped only the box, by adopting a specific shape-grasping configuration (Figure 7.8), while it wasn't possible to find a suitable grasping configuration for any of the other targets. This outcome is expected, as the single-arm setup is not designed for dry conditions and it uses sucker adhesion as its primary grasping mechanism. Conversely, in water, the passive adhesion of the suckers enabled the single arm to secure the other objects as well, even if these large targets are not ideal for a single arm, which is intended to manipulate smaller items in confined spaces. Therefore, the use of multi-arm cooperation demonstrated its effectiveness, providing payload increases ranging from 200% to over 400% compared to the single-arm capabilities within the specific set of evaluated objects.

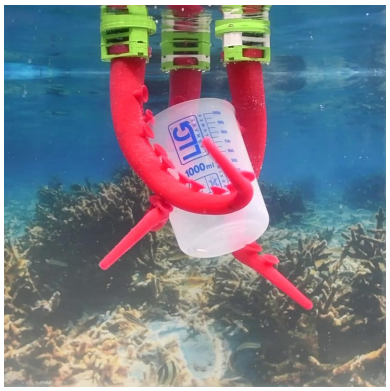

Figure 7.7: Example of "buckling out of the bending plane" phenomenon. The arms suddenly twists sideways instead of compressing the target, resulting in a failed grasp.

Figure 7.8: Successful shape-grasping configuration performed by a single arm to sustain the rectangular box.

Furthermore, with the use of one single arm in an open underwater environment, it can happen that the objects are simply pushed away rather than firmly grasped, if no suckers adhere (Figure 7.9).

(a) (b) (c)

Figure 7.9: Sequence of frames showing a failed grasping attempt by a single arm in an open underwater environment. In (a), the arm makes initial contact with the sphere; in (b), the lack of sucker adhesion causes the bending motion to push the object; in (c), the sphere is displaced away from the arm, preventing a secure grasp.

About the performance of the *Multi-Arm Octopus Robot*, a first comparative analysis can be carried out to explain its distinct behaviors in dry and wet conditions. Testing the system in water requires a specific mass formulation to account for buoyancy. Before adding any payload, each object was filled internally with weights until it reached neutral buoyancy. Consequently, the mass values m reported in Table 7.2 represent the *equivalent mass* added beyond the neutral state. To increase the payload, standardized metallic weights were inserted into the objects, both in air and water. The set consisted of elements with a weight of $200g$, $100g$, $50g$, $20g$, $10g$ and $2g$, in air. Due to the buoyancy force, their effective contribution when submerged is reduced, resulting in masses of $197g$, $98g$, $49g$, $20g$, $10g$, $2g$ (rounded), respectively. These equivalent masses (m_e) added to the system are computed using Equation 7.1 (where ρ_w is the density of the water, V is the volume of the specific metallic weight and m its weight in air). So, for example, a payload of $118g$ was achieved using a $100g$ and a $20g$ weight, in addition to the weights needed to reach neutral buoyancy.

$$m_e = m - \rho_w V \tag{7.1}$$

Comparing the two environments, the tests in water demonstrate a generalized increase in the payload capacity, caused by the engagement of the passive suckers. When operating with three arms, the cooperative action applies opposite forces that compress the object, forcing the suckers against the surface. While a localized study on the exact number

of adhering suckers was not performed, the data still shows a clear trend: in water, by analyzing the midpoints of the recorded payload ranges, an average performance increase of 34.3% was observed when transitioning from air to water. The becher registered the higher improvement percentages in water (up to 75% in L_c – 50% pulling configuration), confirming the excellent adhesion capability of the suckers on smooth surfaces.

To provide a clearer visual representation of the grasping performance, the data relative to the large sphere has been plotted in Figure 7.10, as a significative example. The graphs illustrate the payload capacity as a function of the tendon actuation percentage, comparing the tests in air (left) and water (right). The colored bands represent the payload ranges in the three tested translational positions of the frontal arms ($0.75L_c$, $1.0L_c$, and $1.25L_c$). As evident from the upward shift of the ranges in the right graph, the aquatic environment consistently enhances the payload capabilities of the system across all configurations. Furthermore, the graphs highlight that for a fixed position of the frontal arms, a higher tendon actuation percentage systematically leads to an increased payload capacity; as anticipated, a higher tension allows both greater compression of the object and more effective modeling of the arms around its surface, facilitating also the adhesion of the suckers.

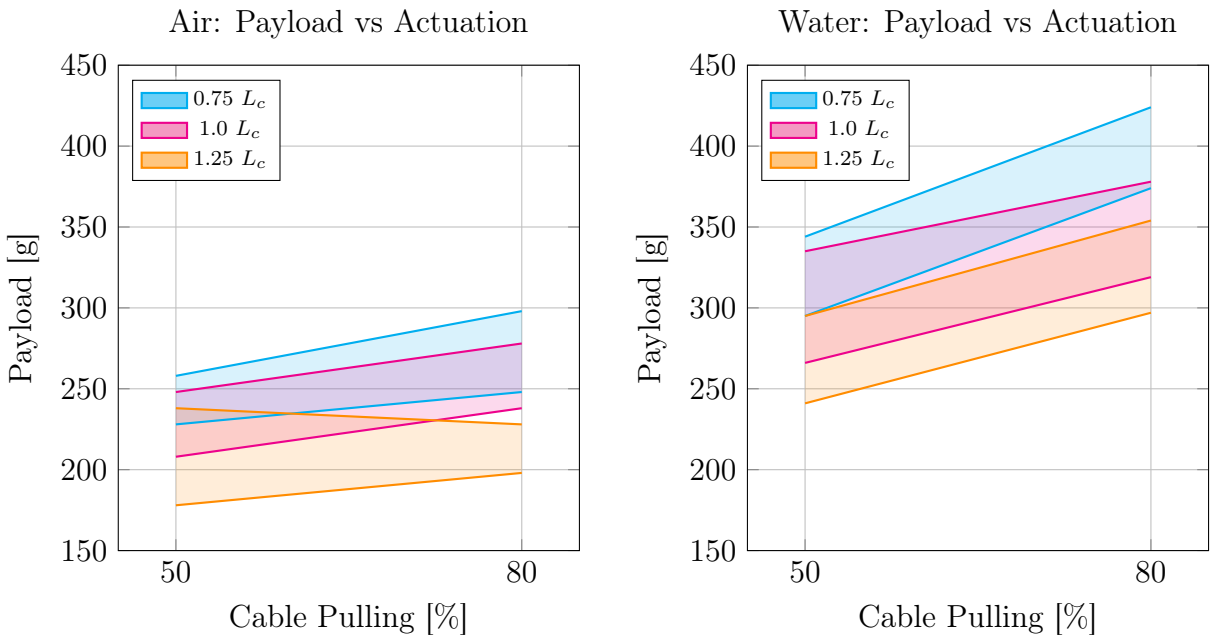

Figure 7.10: Graphical representation of the payload ranges for the large sphere in air (left) and water (right). For each colored volume, under the lower line the grasp is stable, over the upper line the grasp immediately fails, and in between slipping occurs.

The translational DOF plays a crucial role in grasping robustness. As shown in the tables (reading from right to left) and clearly highlighted by the vertical arrangement of the colored bands in the graphs, decreasing the distance between the frontal arms from $1.25L_c$ to $0.75L_c$ always leads to higher payload capacities. In air, a closer distance simply increases the normal compression force, in water, in addition to this, it ensures a more effective orientation of the suckers: at $0.75L_c$, when the ventral cables are pulled, the arms are already in contact with the object, with the ventral side parallel to its surface, allowing an higher number of suckers to adhere properly.

Thanks to the intrinsic softness of the arms, that passively adapt to the surfaces, it was possible to grasp objects with very different geometries (box, spheres, barrel). However, the size of the objects significantly influences the payload capacity observed across the different tests: the robot demonstrated superior grasping performance when grasping large objects (both in air and water) compared to small ones, thanks to the adhesion of more suckers in water, and the bigger surface area available for friction in air. This is evident when comparing the large and small spheres (despite their identical geometry). The small sphere proved extremely difficult to grasp, resulting in the lowest payload values in the tables (up to $78g$ in air and $98g$ in water). The barrel in vertical configuration highlights the power of the setup when dealing with big objects in water, with percentage increases ranging from 26% to 38% with respect to the same object in air. Moreover, it can be grasped even at 50% actuation and L_c distance thanks to suckers, a configuration that completely fails in air. The barrel in horizontal configuration instead has a peculiar behavior: in air the weights that the three arms are able to sustain are bigger than the analogous configurations with the barrel in vertical position; this is due to the fact that one arm penetrates the barrel's top opening, creating a physical constraint that prevents the object from slipping. Additionally, its percentage improvement in water is lower than the one in vertical position (only 9% in $0.75L_c$ - 80% configuration). One exception to these trends can be highlighted: the box grasped with one arm is the only case where the payload capacity in air is higher than in water. This is due to the fact that the grasp of this object with one arm relied purely on friction, which is reduced in wet conditions.

Also the *Basal Grasping* configuration was proven to be effective, but exhibited a lower overall performance compared to *Pinching*. An exception was observed with the box: in this case, the basal grasping outperformed the pinching technique, likely due to the object's pronounced horizontal dimension, that has been handled more effectively with two arms positioned along the horizontal length of the body (Figure 7.12), rather than on the lateral surfaces (Figure 7.11). This is an interesting result, given that in the experimental campaign conducted with the octopus, this grasping strategy was observed

when interacting with long objects, oriented perpendicularly to the axis of the animal (Chapter 4). Finally, although the translational DOF allows the system to grasp objects of different dimensions, in *Basal Grasping* configuration the grasping of smaller items was not successful: in the pinching setup, the frontal arms can close the gap between them, using the ventral bending, while in this setup, the bending direction does not point the opposite arm. Thus, the grasp of objects such as the spheres ($10cm$ and $16cm$) was not effective.

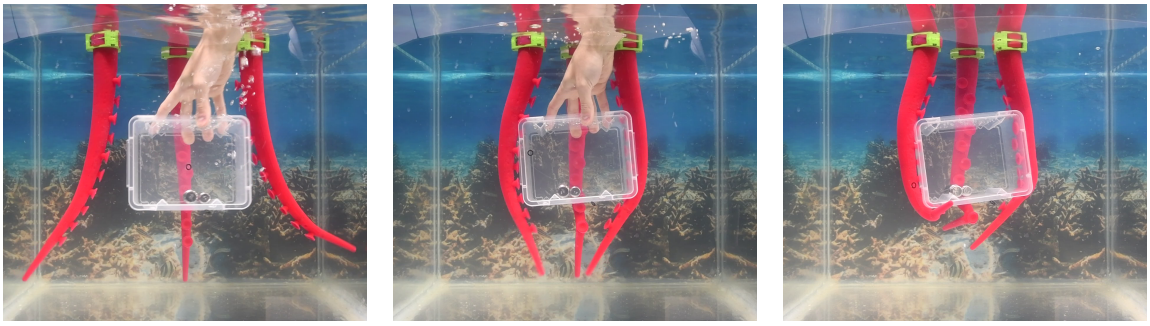

(a) (b) (c)

Figure 7.11: Sequence of frames illustrating the execution of a pinching grasp on the rectangular box, with the frontal arms compressing its lateral surfaces.

(a) (b) (c)

Figure 7.12: Sequence of frames illustrating the execution of a basal grasp on the rectangular box, with the frontal arms that compress the object on its long side, pushing it towards the actuated rear arm.

Although not formally included in the extensive quantitative tables, also the combination of *twisting* and *bending* motions was tested as a complementary grasping strategy. As discussed in Section 7.1, twisting allows the arms to move out of the bending plane of the frontal arms; this was exploited for reaching and securing objects located outside of

this plane (Figure 7.13), demonstrating the multi-arm system's versatility in unstructured scenarios.

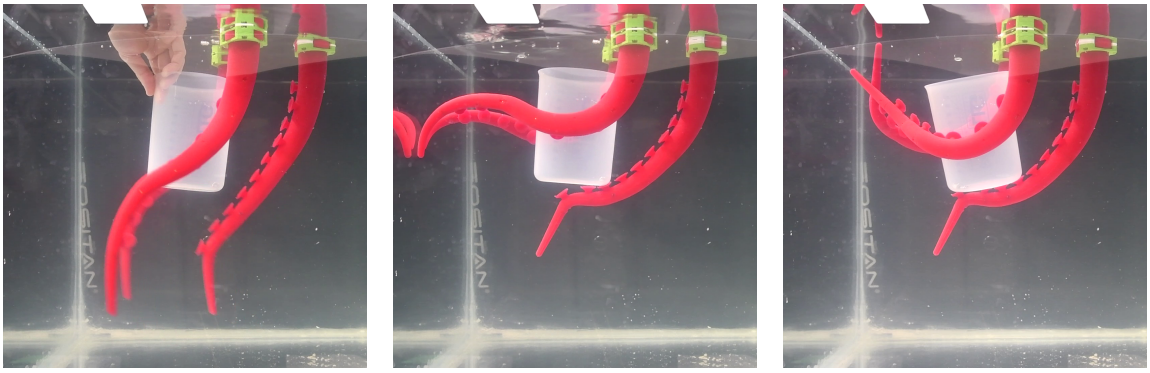

(a) (b) (c)

Figure 7.13: Lateral view of the multi-arm system grasping an out-of-plane object thanks to a combination of twisting and bending motions of the arms.

Finally, to evaluate the mechanical effort required to actuate the soft structure and to derive preliminary considerations on the energy efficiency of the grasping strategies, tensile tests were conducted. A Zwick/Roell Z005 Universal Testing Machine was used to pull the cables associated to the different motions (ventral bending, dorsal bending, and twisting) for both tendon arrangements (Configuration A and Configuration B). The cables were pulled up to their maximum functional stroke of $118mm$. The resulting data are plotted as Force-Displacement curves, which exhibit the typical hysteresis loops associated with the viscoelastic nature of the silicone material (Figure 7.15). Three cycles were recorded for each cable, performed with a speed of $100mm$ per minute.

The maximum force values extracted from these experimental curves provided crucial quantitative data to validate the hardware design. Specifically, the peak forces ($\sim 24N$) recorded at maximum strain, confirmed that the selected motors, capable of delivering a maximum torque of 20.32 $kg \cdot cm$ are adequately sized to actuate the arms. A comparative analysis of the Force-Displacement plots also highlights the differences between the two tendon configurations. As shown in the graphs, the configurations with the anchoring points located further from the base (ventral bending of *Tendon configuration A* and dorsal bending of *Tendon configuration B*) requires a significantly higher pulling force for their actuation, compared to the others (ventral bending of *Tendon configuration B* and dorsal bending of *Tendon configuration A*). This difference is physically consistent: a longer tendon routing implies that a larger volume of silicone material must be compressed during actuation, intrinsically increasing the mechanical resistance of the arm. The increase of the

required pulling force is more pronounced for ventral bending, likely due to the presence of the additional material of the suckers on that side.

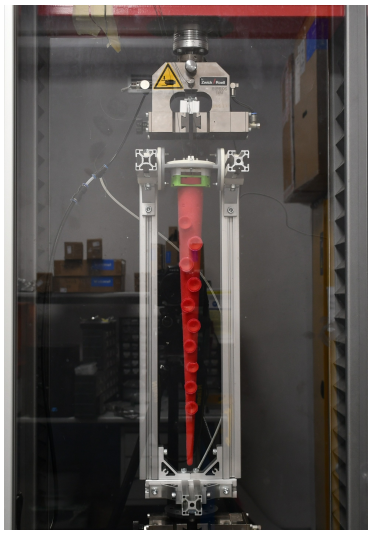

Figure 7.14: Setup for the tensile tests of the arms.

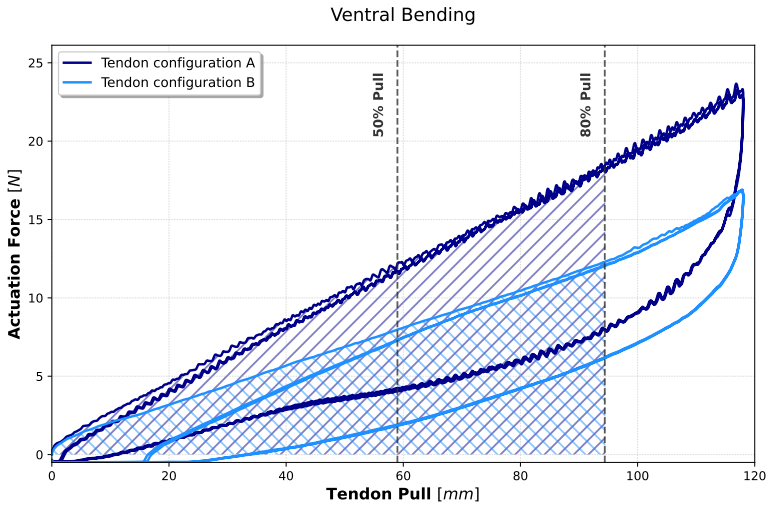

(a)

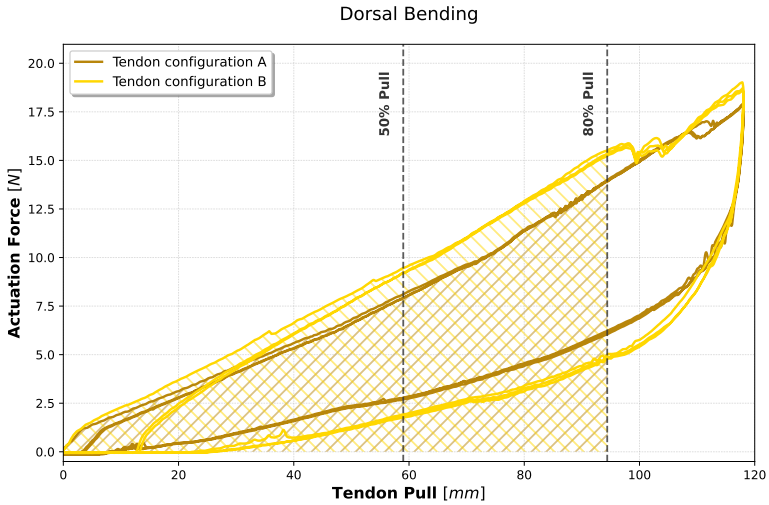

(b)

Figure 7.15: Force-Displacement curves of the arms during (a) ventral and (b) dorsal bending, comparing the two tendon configurations.

These curves also allow for an important consideration regarding the overall energy efficiency of the grasping strategies. In a Force-Displacement plot, the mechanical work done by the motors to pull the cables is represented by the area under the loading curve. As demonstrated in the performance tables (Section 7.2), grasping an object with the arms located at a wider distance (e.g. $1.25L_c$) often requires an 80% tendon actuation to reach

a specific payload capacity. Conversely, from a closer distance ($0.75L_c$) allows the system to secure the same payload with a significantly lower cable pull (e.g. 50%). Translating this to the Force-Displacement plot, reaching an 80% pull requires significantly more mechanical work (a much larger area under the curve) than a 50% pull, due to the non-linear stiffening of the silicone under high compression.

Therefore, the integration of the translational DOF is not only functionally advantageous for adapting to different target sizes, but also energetically convenient. By reducing the gap between the arms, the system minimizes the required tendon stroke, saving in this way a considerable amount of actuation work. The higher the efficiency of the translational DOF's mechanical components, the more significant this energetic advantage becomes. Despite being a 3D-printed prototype, it demonstrated a remarkable degree of mechanical efficiency, proving to be robust enough to withstand the grasping forces and reliable in smoothly adjusting the spacing between the arms. However, since the current is a preliminary setup, a rigorous quantitative efficiency analysis of this specific DOF falls outside the scope of this study; these components will be replaced with optimized, low-friction mechanisms in future iterations.

A similar consideration applies to the motors: while the current consumption during peak actuation was recorded at $1.6A$, this parameter is highly dependent on the specific commercial servos used and could be easily optimized and reduced by adopting more efficient motors.

8 | Conclusions

The objective of this work was to design, develop, and validate a novel bio-inspired robotic system, to address the challenges of underwater grasping of delicate and complex-shaped targets. Building upon previous studies that investigated the performance of a single octopus-inspired arm, this research introduces the cooperative integration of multiple arms, an approach that had never been designed before.

By taking inspiration from the biological strategies observed during the experiments in *Acquario di Genova*, the proposed architecture integrates three soft arms with a translational degree of freedom. This approach successfully overcomes the typical limitations of traditional rigid grippers, which struggle with irregular geometries and risk damaging fragile organisms, as well as the payload constraints of single-arm soft manipulators. The extensive experimental campaign demonstrated the validity and the high effectiveness of the multi-arm cooperative design. The transition from a single-arm setup to the three-arm configuration provided a substantial performance increase, extending the payload capacity by up to 400% within the tested set of objects. Dynamic testing validated the two discovered bio-inspired grasping strategies: *Pinching* and *Basal Grasping*.

The system showed remarkable adaptability across a wide range of targets, effectively exploiting the intrinsic compliance of the silicone structure to secure items without requiring precise geometrical alignment. However, a notable limitation was observed during the interaction with small targets, a challenge that will require further investigation. Furthermore, the experiments highlighted the crucial role of the aquatic environment. The cooperative action of the arms applies opposite compressive forces that naturally force the passive suckers against the object's surface. This engagement proved to be highly effective, leading to an average payload capacity increase of 34.3% in water compared to dry conditions. A key mechanical contribution of this work is the implementation and validation of the translational degree of freedom. Adjusting the initial distance between the frontal arms proved to be fundamental not only for geometrical adaptation to different target sizes but also for overall energy efficiency. As demonstrated by the tensile tests, physically reducing the gap between the arms significantly minimizes the required tendon

stroke to achieve a stable grasp, saving a considerable amount of mechanical actuation work.

The successful validation of this preliminary prototype provides a solid foundation for future engineering refinements. While the PLA rack-and-pinion mechanism proved robust and reliable during the experimental phase, future prototypes will integrate optimized, low-friction transmission mechanisms. Moreover, subsequent iterations will target the hardware optimization of the actuation unit, adopting more efficient commercial servos to significantly minimize current consumption during peak loads. Also the aluminum supporting framework will be optimized to allow its integration and experimental testing on ROVs. Furthermore, while the current system relies exclusively on the intrinsic compliance of the soft silicone to adapt to the target, future work could explore the integration of localized sensory feedback. Embedding tactile or force sensors along the soft arms would allow the system to close the control loop, enabling the robot to autonomously adjust the tendon pulling force based on the perceived stability of the grasp, further enhancing its versatility in unstructured underwater environments, especially in cases where visibility is low or absent. Finally, the transition from a controlled laboratory setup to a fully deployable underwater system requires complete waterproofing of the mechatronic components, an highly challenging phase. These steps are currently being developed for a single arm, with the ultimate goal of conducting experimental validation in a real marine environment, thus opening the path to in-situ biological sampling and delicate manipulation tasks.

Bibliography

[1] F. Ahmed, M. Waqas, B. Shaikh, U. Khan, A. M. Soomro, S. Kumar, H. Ashraf, F. H. Memon, and K. H. Choi. Multi-material Bio-inspired Soft Octopus Robot for Underwater Synchronous Swimming. *Journal of Bionic Engineering*, 19(5):1229–1241, Sept. 2022. ISSN 1672-6529, 2543-2141. doi: 10.1007/s42235-022-00208-x. URL https://link.springer.com/10.1007/s42235-022-00208-x.

[2] A. Arienti, M. Calisti, F. Giorgio-Serchi, and C. Laschi. PoseiDRONE: Design of a soft-bodied ROV with crawling, swimming and manipulation ability.

[3] Y. Bar-Cohen. Biomimetics: biologically inspired technology.

[4] L. Barbieri, F. Bruno, A. Gallo, M. Muzzupappa, and M. L. Russo. Design, prototyping and testing of a modular small-sized underwater robotic arm controlled through a Master-Slave approach. *Ocean Engineering*, 158:253–262, June 2018. ISSN 00298018. doi: 10.1016/j.oceaneng.2018.04.032. URL https://linkinghub.elsevier.com/retrieve/pii/S0029801818304645.

[5] J. Bemfica, C. Melchiorri, L. Moriello, G. Palli, U. Scarcia, and G. Vassura. Mechatronic Design of a Three-Fingered Gripper for Underwater Applications. *IFAC Proceedings Volumes*, 46(5):307–312, 2013. ISSN 14746670. doi: 10.3182/20130410-3-CN-2034.00080. URL https://linkinghub.elsevier.com/retrieve/pii/S1474667015362315.

[6] J. R. Bemfica, C. Melchiorri, L. Moriello, G. Palli, and U. Scarcia. A three-fingered cable-driven gripper for underwater applications. In *2014 IEEE International Conference on Robotics and Automation (ICRA)*, pages 2469–2474, Hong Kong, China, May 2014. IEEE. ISBN 978-1-4799-3685-4. doi: 10.1109/ICRA.2014.6907203. URL http://ieeexplore.ieee.org/document/6907203/.

[7] C. O. Bennice, K. C. Buresch, J. H. Grossman, T. D. Morano, and R. T. Hanlon. Octopus arm flexibility facilitates complex behaviors in diverse natural environments. *Scientific Reports*, 15(1):31875, Sept. 2025. ISSN 2045-

2322. doi: 10.1038/s41598-025-10674-y. URL https://www.nature.com/articles/s41598-025-10674-y.

[8] K. Bezha and K. Ito. Soft manipulator inspired by octopi: object grasping in all anatomical planes using a tendon-driven continuum arm. *Artificial Life and Robotics*, 28(1):96–105, Feb. 2023. ISSN 1433-5298, 1614-7456. doi: 10.1007/s10015-022-00844-w. URL https://link.springer.com/10.1007/s10015-022-00844-w.

[9] F. Bidel, N. C. Bennett, and T. J. Wardill. Octopus bimaculoides' arm recruitment and use during visually evoked prey capture. *Current Biology*, 32(21): 4727–4733.e3, Nov. 2022. ISSN 09609822. doi: 10.1016/j.cub.2022.08.080. URL https://linkinghub.elsevier.com/retrieve/pii/S0960982222014026.

[10] A. Biewener, R. M. Alexander, and N. C. Heglund. Elastic energy storage in the hopping of kangaroo rats *(Dipodomys spectabilis)*. *Journal of Zoology*, 195(3):369–383, Nov. 1981. ISSN 0952-8369, 1469-7998. doi: 10.1111/j.1469-7998.1981.tb03471.x. URL https://zslpublications.onlinelibrary.wiley.com/doi/10.1111/j.1469-7998.1981.tb03471.x.

[11] K. C. Buresch, K. Sklar, J. Y. Chen, S. R. Madden, A. S. Mongil, G. V. Wise, J. G. Boal, and R. T. Hanlon. Contact chemoreception in multi-modal sensing of prey by Octopus. *Journal of Comparative Physiology A*, 208(3):435–442, May 2022. ISSN 0340-7594, 1432-1351. doi: 10.1007/s00359-022-01549-y. URL https://link.springer.com/10.1007/s00359-022-01549-y.

[12] K. C. Buresch, N. D. Huget, W. C. Brister, E. Y. Zhou, A. S. Lineaweaver, C. Rifai, J. Hu, Z. E. Stevenson, J. G. Boal, and R. T. Hanlon. Evidence for tactile 3D shape discrimination by octopus. *Journal of Comparative Physiology A*, 210(5):815–823, Sept. 2024. ISSN 0340-7594, 1432-1351. doi: 10.1007/s00359-024-01696-4. URL https://link.springer.com/10.1007/s00359-024-01696-4.

[13] R. A. Byrne, M. J. Kuba, D. V. Meisel, U. Griebel, and J. A. Mather. Octopus arm choice is strongly influenced by eye use. *Behavioural Brain Research*, 172(2): 195–201, Sept. 2006. ISSN 01664328. doi: 10.1016/j.bbr.2006.04.026. URL https://linkinghub.elsevier.com/retrieve/pii/S0166432806002439.

[14] M. Calisti, A. Arienti, F. Renda, G. Levy, B. Hochner, B. Mazzolai, P. Dario, and C. Laschi. Design and development of a soft robot with crawling and grasping capabilities. In *2012 IEEE International Conference on Robotics and Automation*, pages 4950–4955, St Paul, MN, USA, May 2012. IEEE. ISBN 978-1-4673-1405-3 978-1-

4673-1403-9 978-1-4673-1578-4 978-1-4673-1404-6. doi: 10.1109/ICRA.2012.6224671. URL http://ieeexplore.ieee.org/document/6224671/.

[15] M. Cianchetti, A. Arienti, M. Follador, B. Mazzolai, P. Dario, and C. Laschi. Design concept and validation of a robotic arm inspired by the octopus. *Materials Science and Engineering: C*, 31(6):1230–1239, Aug. 2011. ISSN 09284931. doi: 10.1016/j.msec.2010.12.004. URL https://linkinghub.elsevier.com/retrieve/pii/S0928493110003450.

[16] M. Cianchetti, M. Follador, B. Mazzolai, P. Dario, and C. Laschi. Design and development of a soft robotic octopus arm exploiting embodied intelligence. In *2012 IEEE International Conference on Robotics and Automation*, pages 5271–5276, St Paul, MN, USA, May 2012. IEEE. ISBN 978-1-4673-1405-3 978-1-4673-1403-9 978-1-4673-1578-4 978-1-4673-1404-6. doi: 10.1109/ICRA.2012.6224696. URL http://ieeexplore.ieee.org/document/6224696/.

[17] N. El-Atab, R. B. Mishra, F. Al-Modaf, L. Joharji, A. A. Alsharif, H. Alamoudi, M. Diaz, N. Qaiser, and M. M. Hussain. Soft Actuators for Soft Robotic Applications: A Review. *Advanced Intelligent Systems*, 2(10):2000128, Oct. 2020. ISSN 2640-4567, 2640-4567. doi: 10.1002/aisy.202000128. URL https://advanced.onlinelibrary.wiley.com/doi/10.1002/aisy.202000128.

[18] J. J. Fernandez, M. Prats, P. J. Sanz, J. C. Garcia, R. Marin, M. Robinson, D. Ribas, and P. Ridao. Grasping for the Seabed: Developing a New Underwater Robot Arm for Shallow-Water Intervention. *IEEE Robotics & Automation Magazine*, 20(4):121–130, Dec. 2013. ISSN 1070-9932. doi: 10.1109/MRA.2013.2248307. URL http://ieeexplore.ieee.org/document/6627980/.

[19] G. Fiorito, A. Affuso, J. Basil, A. Cole, P. De Girolamo, L. D'Angelo, L. Dickel, C. Gestal, F. Grasso, M. Kuba, F. Mark, D. Melillo, D. Osorio, K. Perkins, G. Ponte, N. Shashar, D. Smith, J. Smith, and P. L. Andrews. Guidelines for the Care and Welfare of Cephalopods in Research –A consensus based on an initiative by CephRes, FELASA and the Boyd Group. *Laboratory Animals*, 49(2_suppl):1–90, Oct. 2015. ISSN 0023-6772, 1758-1117. doi: 10.1177/0023677215580006. URL https://journals.sagepub.com/doi/10.1177/0023677215580006.

[20] K. C. Galloway, K. P. Becker, B. Phillips, J. Kirby, S. Licht, D. Tchernov, R. J. Wood, and D. F. Gruber. Soft Robotic Grippers for Biological Sampling on Deep Reefs.

[21] A. J. Gendreau, C. Boucaud, K. C. Buresch, A. S. Rooney, H. Morris, and R. T.

Hanlon. How octopuses use and recruit additional arms to find and manipulate visually hidden items. *Biology Open*, 14(7):bio062011, July 2025. ISSN 2046-6390. doi: 10.1242/bio.062011. URL https://journals.biologists.com/bio/article/14/7/bio062011/368537/How-octopuses-use-and-recruit-additional-arms-to.

[22] S. Hanassy, A. Botvinnik, T. Flash, and B. Hochner. Stereotypical reaching movements of the octopus involve both bend propagation and arm elongation. *Bioinspiration & Biomimetics*, 10(3):035001, May 2015. ISSN 1748-3190. doi: 10.1088/1748-3190/10/3/035001. URL https://iopscience.iop.org/article/10.1088/1748-3190/10/3/035001.

[23] Y. Hao, Z. Gong, Z. Xie, S. Guan, X. Yang, T. Wang, and L. Wen. A Soft Bionic Gripper with Variable Effective Length. *Journal of Bionic Engineering*, 15(2):220–235, Mar. 2018. ISSN 1672-6529, 2543-2141. doi: 10.1007/s42235-018-0017-9. URL http://link.springer.com/10.1007/s42235-018-0017-9.

[24] D. Herrero-Pérez and H. Martínez-Barberá. Soft Gripper Design and Fabrication for Underwater Grasping. *Applied Sciences*, 12(21):10694, Oct. 2022. ISSN 2076-3417. doi: 10.3390/app122110694. URL https://www.mdpi.com/2076-3417/12/21/10694.

[25] H. Huang, Q. Tang, J. Li, W. Zhang, X. Bao, H. Zhu, and G. Wang. A review on underwater autonomous environmental perception and target grasp, the challenge of robotic organism capture. *Ocean Engineering*, 195:106644, Jan. 2020. ISSN 00298018. doi: 10.1016/j.oceaneng.2019.106644. URL https://linkinghub.elsevier.com/retrieve/pii/S0029801819307644.

[26] J. Hughes, U. Culha, F. Giardina, F. Guenther, A. Rosendo, and F. Iida. Soft Manipulators and Grippers: A Review. *Frontiers in Robotics and AI*, 3, Nov. 2016. ISSN 2296-9144. doi: 10.3389/frobt.2016.00069. URL http://journal.frontiersin.org/article/10.3389/frobt.2016.00069/full.

[27] K. Ito and S. Hagimori. Flexible manipulator inspired by octopus: development of soft arms using sponge and experiment for grasping various objects. *Artificial Life and Robotics*, 22(3):283–288, Sept. 2017. ISSN 1433-5298, 1614-7456. doi: 10.1007/s10015-017-0360-7. URL http://link.springer.com/10.1007/s10015-017-0360-7.

[28] R. Janardhana, F. Akram, Z. Guler, A. Adaval, and N. Jackson. A Comprehensive Experimental, Simulation, and Characterization Mechanical Analysis of Ecoflex and Its Formulation Under Uniaxial Testing. *Materials*, 18(13):3037, June 2025. ISSN

1996-1944. doi: 10.3390/ma18133037. URL https://www.mdpi.com/1996-1944/18/13/3037.

[29] H. Jiang, X. Han, Y. Jing, N. Guo, F. Wan, and C. Song. Rigid–Soft Interactive Design of a Lobster-Inspired Finger Surface for Enhanced Grasping Underwater. *Frontiers in Robotics and AI*, 8:787187, Dec. 2021. ISSN 2296-9144. doi: 10.3389/frobt.2021.787187. URL https://www.frontiersin.org/articles/10.3389/frobt.2021.787187/full.

[30] S. Kim, C. Laschi, and B. Trimmer. Soft robotics: a bioinspired evolution in robotics. *Trends in Biotechnology*, 31(5):287–294, May 2013. ISSN 01677799. doi: 10.1016/j.tibtech.2013.03.002. URL https://linkinghub.elsevier.com/retrieve/pii/S0167779913000632.

[31] C. Laschi, B. Mazzolai, V. Mattoli, M. Cianchetti, and P. Dario. Design of a biomimetic robotic octopus arm. *Bioinspiration & Biomimetics*, 4(1):015006, Mar. 2009. ISSN 1748-3182, 1748-3190. doi: 10.1088/1748-3182/4/1/015006. URL https://iopscience.iop.org/article/10.1088/1748-3182/4/1/015006.

[32] C. Laschi, B. Mazzolai, and M. Cianchetti. Soft robotics: Technologies and systems pushing the boundaries of robot abilities. *Science Robotics*, 1(1):eaah3690, Dec. 2016. ISSN 2470-9476. doi: 10.1126/scirobotics.aah3690. URL https://www.science.org/doi/10.1126/scirobotics.aah3690.

[33] C. Laschi, J. Rossiter, F. Iida, M. Cianchetti, and L. Margheri, editors. *Soft Robotics: Trends, Applications and Challenges*, volume 17 of *Biosystems & Biorobotics*. Springer International Publishing, Cham, 2017. doi: 10.1007/978-3-319-46460-2.

[34] S. Leanza, J. Lu-Yang, B. Kaczmarski, S. Wu, E. Kuhl, and R. R. Zhao. Elephant Trunk Inspired Multimodal Deformations and Movements of Soft Robotic Arms. *Advanced Functional Materials*, 34(29):2400396, July 2024. ISSN 1616-301X, 1616-3028. doi: 10.1002/adfm.202400396. URL https://advanced.onlinelibrary.wiley.com/doi/10.1002/adfm.202400396.

[35] J. Lemburg, P. Kampmann, and F. Kirchner. A small-scale actuator with passive-compliance for a fine-manipulation deep-sea manipulator. In *OCEANS'11 MTS/IEEE KONA*, pages 1–4, Waikoloa, HI, Sept. 2011. IEEE. ISBN 978-1-4577-1427-6 978-0-933957-39-8. doi: 10.23919/OCEANS.2011.6107012. URL http://ieeexplore.ieee.org/document/6107012/.

[36] J. Liu, S. Iacoponi, C. Laschi, L. Wen, and M. Calisti. Underwater Mobile Manipulation: A Soft Arm on a Benthic Legged Robot. *IEEE Robotics & Automation*

Magazine, 27(4):12–26, Dec. 2020. ISSN 1070-9932, 1558-223X. doi: 10.1109/MRA.2020.3024001. URL https://ieeexplore.ieee.org/document/9216533/.

[37] L. Margheri, C. Laschi, and B. Mazzolai. Soft robotic arm inspired by the octopus: I. From biological functions to artificial requirements. *Bioinspiration & Biomimetics*, 7(2):025004, June 2012. ISSN 1748-3182, 1748-3190. doi: 10.1088/1748-3182/7/2/025004. URL https://iopscience.iop.org/article/10.1088/1748-3182/7/2/025004.

[38] M. Martini, G. Pei, Y. Ansari, E. Solfiti, J. Hughes, and B. Mazzolai. Towards the Benchmarking of Embodied Sensors for Pose Tracking in Octopus-Inspired Robotic Arms. .

[39] M. Martini, E. Solfiti, A. Mondini, E. D. Dottore, A. Parmiggiani, E. Sinibaldi, and B. Mazzolai. Routing Optimization of Cable-driven Octopus-inspired Manipulators with Minimal Actuation via Genetic Algorithm and Finite Element Method. .

[40] A. Mazzeo, J. Aguzzi, M. Calisti, S. Canese, F. Vecchi, S. Stefanni, and M. Controzzi. Marine Robotics for Deep-Sea Specimen Collection: A Systematic Review of Underwater Grippers. *Sensors*, 22(2):648, Jan. 2022. ISSN 1424-8220. doi: 10.3390/s22020648. URL https://www.mdpi.com/1424-8220/22/2/648.

[41] B. Mazzolai, C. Laschi, M. Cianchetti, F. Patane, L. Bassi-Luciani, I. Izzo, and P. Dario. Biorobotic Investigation on the Muscle Structure of an Octopus Tentacle. In *2007 29th Annual International Conference of the IEEE Engineering in Medicine and Biology Society*, pages 1471–1474, Lyon, France, Aug. 2007. IEEE. ISBN 978-1-4244-0787-3 978-1-4244-0788-0. doi: 10.1109/IEMBS.2007.4352578. URL http://ieeexplore.ieee.org/document/4352578/. ISSN: 1557-170X.

[42] B. Mazzolai, A. Mondini, F. Tramacere, and E. D. Dottore. Octopus-inspired Technologies for Grasping and Manipulation Tasks. Oct. 2019. doi: 10.5281/ZENODO.4783760. URL https://zenodo.org/record/4783760. Publisher: Zenodo.

[43] B. Mazzolai, A. Mondini, F. Tramacere, G. Riccomi, A. Sadeghi, G. Giordano, E. Del Dottore, M. Scaccia, M. Zampato, and S. Carminati. Octopus-Inspired Soft Arm with Suction Cups for Enhanced Grasping Tasks in Confined Environments. *Advanced Intelligent Systems*, 1(6):1900041, Oct. 2019. ISSN 2640-4567, 2640-4567. doi: 10.1002/aisy.201900041. URL https://onlinelibrary.wiley.com/doi/10.1002/aisy.201900041.

[44] R. R. Murphy. *Disaster Robotics*. The MIT Press, Cambridge, MA, 2014.

[45] G. Palli, L. Moriello, and C. Melchiorri. Performance and Sealing Material Evaluation in 6-axis Force-Torque Sensors for Underwater Robotics. *IFAC-PapersOnLine*, 48 (2):177–182, 2015. ISSN 24058963. doi: 10.1016/j.ifacol.2015.06.029. URL https://linkinghub.elsevier.com/retrieve/pii/S2405896315002682.

[46] G. Palli, L. Moriello, U. Scarcia, and C. Melchiorri. An Underwater Robotic Gripper with Embedded Force/Torque Wrist Sensor. *IFAC-PapersOnLine*, 50(1): 11209–11214, July 2017. ISSN 24058963. doi: 10.1016/j.ifacol.2017.08.2095. URL https://linkinghub.elsevier.com/retrieve/pii/S2405896317327556.

[47] R. Pfeifer and J. C. Bongard. *How the Body Shapes the Way We Think: A New View of Intelligence*. The MIT Press, Cambridge, MA, 2007.

[48] R. Pfeifer, M. Lungarella, and F. Iida. Self-organization, embodiment, and biologically inspired robotics. *Science*, 318(5853):1088–1093, 2007. doi: 10.1126/science.1145803.

[49] G. Picardi, M. De Luca, G. Chimienti, M. Cianchetti, and M. Calisti. User-Driven Design and Development of an Underwater Soft Gripper for Biological Sampling and Litter Collection. *Journal of Marine Science and Engineering*, 11(4):771, Mar. 2023. ISSN 2077-1312. doi: 10.3390/jmse11040771. URL https://www.mdpi.com/2077-1312/11/4/771.

[50] P. Polygerinos, N. Correll, S. A. Morin, B. Mosadegh, C. D. Onal, K. Petersen, M. Cianchetti, M. T. Tolley, and R. F. Shepherd. Soft Robotics: Review of Fluid-Driven Intrinsically Soft Devices; Manufacturing, Sensing, Control, and Applications in Human-Robot Interaction. *Advanced Engineering Materials*, 19(12):1700016, Dec. 2017. ISSN 1438-1656, 1527-2648. doi: 10.1002/adem.201700016. URL https://advanced.onlinelibrary.wiley.com/doi/10.1002/adem.201700016.

[51] D. Rus and M. T. Tolley. Design, fabrication and control of soft robots. *Nature*, 521 (7553):467–475, May 2015. ISSN 0028-0836, 1476-4687. doi: 10.1038/nature14543. URL https://www.nature.com/articles/nature14543.

[52] N. Simaan. Snake-Like Units Using Flexible Backbones and Actuation Redundancy for Enhanced Miniaturization. In *Proceedings of the 2005 IEEE International Conference on Robotics and Automation*, pages 3012–3017, Barcelona, Spain, 2005. IEEE. ISBN 978-0-7803-8914-4. doi: 10.1109/ROBOT.2005.1570572. URL http://ieeexplore.ieee.org/document/1570572/.

[53] N. R. Sinatra, C. B. Teeple, D. M. Vogt, K. K. Parker, D. F. Gruber, and R. J. Wood. Ultragentle manipulation of delicate structures using a soft robotic gripper. *Science*

Robotics, 4(33):eaax5425, Aug. 2019. ISSN 2470-9476. doi: 10.1126/scirobotics.aax5425. URL https://www.science.org/doi/10.1126/scirobotics.aax5425.

[54] D. M. Sivitilli, T. Strong, W. Weertman, J. Ullmann, J. R. Smith, and D. H. Gire. Mechanisms of octopus arm search behavior without visual feedback. *Bioinspiration & Biomimetics*, 18(6):066017, Nov. 2023. ISSN 1748-3182, 1748-3190. doi: 10.1088/1748-3190/ad0013. URL https://iopscience.iop.org/article/10.1088/1748-3190/ad0013.

[55] D. M. Sivitilli, A. Zulch, and D. H. Gire. Octopus arm search strategies over complex surfaces, Aug. 2023. URL http://biorxiv.org/lookup/doi/10.1101/2023.07.31.551380.

[56] S. Sivčev, J. Coleman, E. Omerdić, G. Dooly, and D. Toal. Underwater manipulators: A review. *Ocean Engineering*, 163:431–450, Sept. 2018. ISSN 00298018. doi: 10.1016/j.oceaneng.2018.06.018. URL https://linkinghub.elsevier.com/retrieve/pii/S0029801818310308.

[57] E. Solfiti, A. Mondini, E. D. Dottore, B. Mazzolai, and A. Parmiggiani. Soft 3D-Printed Endoskeleton for Precise Tendon Routing in Soft Robotics. *IEEE Robotics and Automation Letters*, 11(2):2282–2289, Feb. 2026. ISSN 2377-3766, 2377-3774. doi: 10.1109/LRA.2025.3648604. URL https://ieeexplore.ieee.org/document/11315156/.

[58] SpiderWire. Shop All Durabraid Series | SpiderWire. https://www.spiderwire.com. [Online; accessed 28-01-2026].

[59] H. Stuart, S. Wang, O. Khatib, and M. R. Cutkosky. The Ocean One hands: An adaptive design for robust marine manipulation. *The International Journal of Robotics Research*, 36(2):150–166, Feb. 2017. ISSN 0278-3649, 1741-3176. doi: 10.1177/0278364917694723. URL https://journals.sagepub.com/doi/10.1177/0278364917694723.

[60] H. S. Stuart, S. Wang, B. Gardineer, D. L. Christensen, D. M. Aukes, and M. Cutkosky. A compliant underactuated hand with suction flow for underwater mobile manipulation. In *2014 IEEE International Conference on Robotics and Automation (ICRA)*, pages 6691–6697, Hong Kong, May 2014. IEEE. ISBN 978-1-4799-3685-4. doi: 10.1109/ICRA.2014.6907847. URL https://ieeexplore.ieee.org/document/6907847/.

[61] G. Sumbre, G. Fiorito, T. Flash, and B. Hochner. Octopuses Use a Human-like Strategy to Control Precise Point-to-Point Arm Movements. *Current Biology*, 16(8):

767–772, Apr. 2006. ISSN 09609822. doi: 10.1016/j.cub.2006.02.069. URL https://linkinghub.elsevier.com/retrieve/pii/S0960982206012747.

[62] D. Trivedi, C. D. Rahn, W. M. Kier, and I. D. Walker. Soft Robotics: Biological Inspiration, State of the Art, and Future Research. *Applied Bionics and Biomechanics*, 5 (3):99–117, Jan. 2008. ISSN 1176-2322, 1754-2103. doi: 10.1080/11762320802557865. URL https://onlinelibrary.wiley.com/doi/10.1080/11762320802557865.

[63] D. M. Vogt, K. P. Becker, B. T. Phillips, M. A. Graule, R. D. Rotjan, T. M. Shank, E. E. Cordes, R. J. Wood, and D. F. Gruber. Shipboard design and fabrication of custom 3D-printed soft robotic manipulators for the investigation of delicate deep-sea organisms. *PLOS ONE*, 13(8):e0200386, Aug. 2018. ISSN 1932-6203. doi: 10.1371/journal.pone.0200386. URL https://dx.plos.org/10.1371/journal.pone.0200386.

[64] H. Wang, X. Huang, X. Qi, and Q. Meng. Development of Underwater Robot Hand and Its Finger Tracking Control. In *2007 IEEE International Conference on Automation and Logistics*, pages 2973–2977, Jinan, China, Aug. 2007. IEEE. ISBN 978-1-4244-1530-4 978-1-4244-1531-1. doi: 10.1109/ICAL.2007.4339091. URL http://ieeexplore.ieee.org/document/4339091/.

[65] M. Wu, X. Zheng, R. Liu, N. Hou, W. H. Afridi, R. H. Afridi, X. Guo, J. Wu, C. Wang, and G. Xie. Glowing Sucker Octopus (*Stauroteuthis syrtensis*)-Inspired Soft Robotic Gripper for Underwater Self-Adaptive Grasping and Sensing. *Advanced Science*, 9(17):2104382, June 2022. ISSN 2198-3844, 2198-3844. doi: 10.1002/advs.202104382. URL https://advanced.onlinelibrary.wiley.com/doi/10.1002/advs.202104382.

[66] M. Wu, W. H. Afridi, J. Wu, R. H. Afridi, K. Wang, X. Zheng, C. Wang, and G. Xie. Octopus-Inspired Underwater Soft Robotic Gripper with Crawling and Swimming Capabilities. *Research*, 7:0456, Jan. 2024. ISSN 2639-5274. doi: 10.34133/research.0456. URL https://spj.science.org/doi/10.34133/research.0456.

[67] M. S. Xavier, C. D. Tawk, A. Zolfagharian, J. Pinskier, D. Howard, T. Young, J. Lai, S. M. Harrison, Y. K. Yong, M. Bodaghi, and A. J. Fleming. Soft Pneumatic Actuators: A Review of Design, Fabrication, Modeling, Sensing, Control and Applications. *IEEE Access*, 10:59442–59485, 2022. ISSN 2169-3536. doi: 10.1109/ACCESS.2022.3179589. URL https://ieeexplore.ieee.org/document/9785890/.

[68] T. Ye, Y. Wang, S. Xu, Y. Wang, and J. Li. Modeling and motion control of an octopus-like flexible manipulator actuated by shape memory alloy wires. *Journal of*

Intelligent Material Systems and Structures, 33(1):3–16, Jan. 2022. ISSN 1045-389X, 1530-8138. doi: 10.1177/1045389X211023579. URL https://journals.sagepub.com/doi/10.1177/1045389X211023579.

[69] B. Zhang, Y. Zhang, Y. Li, S. Xuan, H. W. Ng, Y. Liufu, Z. Tang, and C. Laschi. Octopus-Swimming-Like Robot with Soft Asymmetric Arms. In *2025 IEEE 8th International Conference on Soft Robotics (RoboSoft)*, pages 1–8, Apr. 2025. doi: 10.1109/RoboSoft63089.2025.11020919. URL http://arxiv.org/abs/2410.11764. arXiv:2410.11764 [cs].

[70] J. Zhou, Y. Chen, Y. Hu, Z. Wang, Y. Li, G. Gu, and Y. Liu. Adaptive Variable Stiffness Particle Phalange for Robust and Durable Robotic Grasping. *Soft Robotics*, 7(6):743–757, Dec. 2020. ISSN 2169-5172, 2169-5180. doi: 10.1089/soro.2019.0089. URL https://www.liebertpub.com/doi/10.1089/soro.2019.0089.

Acknowledgements

I would like to deeply thank my advisor, Giovanni Bianchi, for his support during the development of this work. My thanks also go to my co-advisors, Barbara Mazzolai and Emanuele Solfiti, for their constant guidance and for giving me the opportunity to work on this fascinating project. A special thanks goes to the staff at *IIT*, with a particular mention to Alessio, for his fundamental assistance and technical support. Finally, I would like to thank the biologists of *Acquario di Genova*, Laura, Alessandra, and Giacomo, for sharing their expertise and making the biological investigation possible.